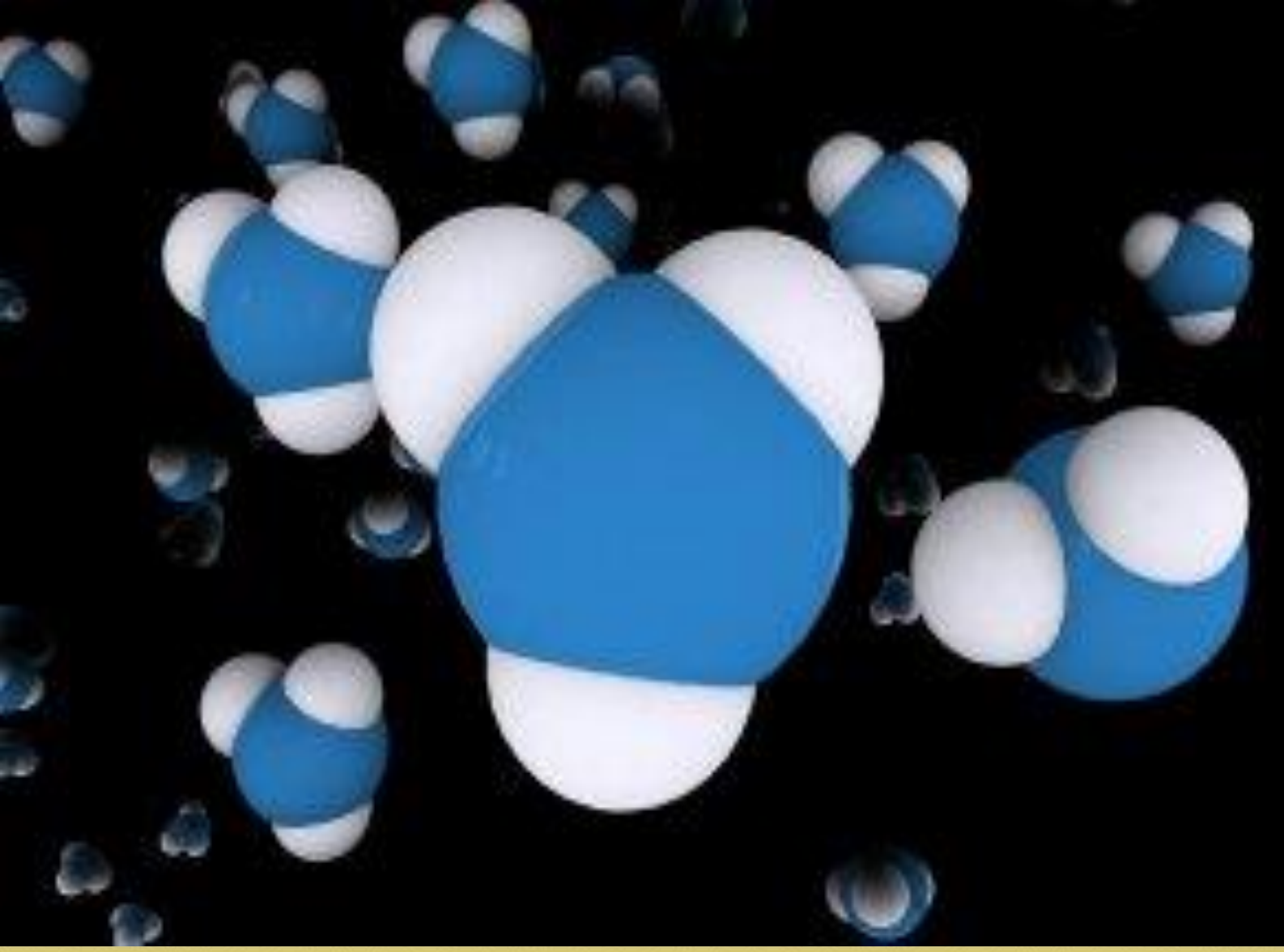

José Manuel Carvalheiro Perdigoto

Measurement of ion mobility in relevant mixtures used in gas detectors

Master's thesis in the scientific area of Physics Engineering, supervised by Professor Doctor Filipa Isabel Gouveia de Melo Borges Belo Soares and Master André Filipe Ventura Cortez and submitted to the Department of Physics, Faculty of Science and Technology, University of Coimbra

September 2017

UNIVERSIDADE DE COIMBRA

UNIVERSITY OF COIMBRA

Measurement of ion mobility in relevant mixtures used in gas detectors

José Manuel Carvalheiro Perdigoto

Dissertation for MSc degree in Physics Engineering supervised by
Prof. Dr. FILIPA ISABEL G. DE MELO BORGES BELO SOARES
MSc. ANDRÉ FILIPE VENTURA CORTEZ

in the
FACULTY OF SCIENCE AND TECHNOLOGY
DEPARTMENT OF PHYSICS

2017

Acknowledgements

First of all I want to thank Professor Doctor Filipa Borges, who supervised this dissertation, for the constant help and support provided throughout this project. Your guidance at key moments in my work was essential to attain the objectives outlined.

To Engineer André Cortez, who co-supervised this work, for his expertise, who was always available to answer to all the questions that I had during the project, allowing me to work independently for the majority of time.

To Professor Doctor Carlos Conde, for the time spared acompanying the progress of the work, while providing valuable advices.

To Professor Doctor Rob Veenhof who was a key part on solving some questions regarding the identification of some ions in the experiment, allowing the fluent progress of the work.

To all elements in the LIP Coimbra staff for providing with their knowledge and wisdom, an important experience in my life.

To all my friends, who were a solid support throughout this journey and for being a distraction from work when it was needed.

To my famiy, I thank for their love, patience and support during all these years.

Abstract

Transition Radiation Detectors (TRDs) are mainly used for particle identification at high momenta. Moreover, the choice of the gas mixture for such detectors is determined by several parameters such as high electron/ion velocity and low electron diffusion, which are of key importance as they influence the rate capability and signal formation of detectors such as the Multi-Wire Proportional Chambers (MWPCs).

In the span of our participation in the RD51 collaboration/CERN, a common project was established with GSI Darmstag (Germany), Uludağ University (Turkey) and VECC (India) regarding the study of ion transport properties of relevant gas mixtures for ALICE TPC. With this in mind, we performed experimental ion mobility measurements, K_0, for several gas mixtures, namely xenon mixtures (Xe-C_2H_6 and Xe-CH_4) and nitrogen mixtures (Ar-N_2). The results are presented for total pressures ranging from 6-10 Torr and for reduced electric fields (E/N) in the 10-25 Td range at room temperature.

The IDC (Ion Drift Chamber) used to conduct the ion mobility studies was initially developed by P. N. B. Neves [4]. The techniques to perform the aforementioned studies are described in this report and make use of a Gaseous ElectronMultiplier (GEM) and a UV flash lamp to produce the ions.

The results for the Xe-C_2H_6 mixtures show the presence of two peaks throughout the entire range studied, besides the appearance of a small bump at the right side of the main peak for concentrations of Xe higher than 70% and reduced electric fields higher than 20 Td. While for the Xe-CH_4 mixtures it is reported the presence of two distinct groups of ions, with their nature depending on the mixture ratio since they are originated by both Xe and CH_4.

Keywords: Charge transport and multiplication in gas; Ion sources (positive ions, negative ions); Gaseous detectors; Ionization and excitation processes; Ion mobility.

Resumo

Os TRD (Detetores de Radiação de Transição) são maioritariamente usados na identificação de partículas de elevado momento linear. Nesta base, a escolha da mistura gasosa para tais detetores é determinada por parâmetros, como a elevada velocidade de eletrões/iões e baixa difusão de eletrões, os quais são de extrema importância já que influenciam a taxa de aquisição e a formação de sinal de detetores como as Câmaras Proporcionais de Multi-Fios (MWPCs).

No contexto da nossa participação na colaboração RD51/CERN, foi estabelecido um projeto comum com a GSI Darmstag (Alemanha), Universidade de Uludağ (Turquia) e VECC (India) que se focou no estudo de propriedades de transporte de iões de misturas gasosas relevantes para o ALICE TPC. Tendo isso como foco, foram efetuadas medidas experimentais de mobilidade reduzida de iões, K_0, para várias misturas gasosas, nomeadamente para misturas de Xenon (Xe-C_2H_6 and Xe-CH_4) e misturas de azoto (Ar-N_2). Os resultados são apresentados para pressões totais de 8 Torr e campos elétricos reduzidos (E/N) compreendidos entre 10 - 25 Td, à temperatura ambiente.

A IDC ("Ion Drift Chamber") usada para efetuar os estudos de mobilidade de iões foi inicialmente desenvolvida por P.N.B. Neves. As técnicas para a realização dos estudos anteriormente mencionados são descritas neste documento e fazem uso de um GEM ("Gaseous Electron Multiplier") e uma lâmpada de flash UV para produzir os iões.

Os resultados relativos a misturas com Xe-C_2H_6 revelam a presença de dois picos ao longo de todo o estudo efetuado, para além do aparecimento de um pequeno pico à direita do pico principal para concentrações de Xe superiores a 70% e campos reduzidos de 20 Td. Já para misturas de Xe-CH_4 é reportado a presença de dois grupos distintos de iões, em que a natureza dos mesmos depende do rácio da mistura, já que estes são originados tanto por Xe como por CH_4.

Keywords: Transporte de cargas e multiplicação em gases; Fontes de iões (iões

positivos, iões negativos), Detetores gasosos; Processos de ionização e excitação; Mobilidade de iões.

Publications

Scientific Papers

1. J.M.C. Perdigoto *et al*, "Experimental ion mobility measurements in Xe-CH_4", *Journal of Instrumentation*, *vol.12* P09003, 2017- published

2. J.M.C. Perdigoto *et al* "Experimental ion mobility measurements in Xe-C_2H_6"- to be published

Oral Communications

3. J.M.C. Perdigoto *et al*, "RD51 Collaboration - Ion transport in Xe-CO_2 mixtures", oral presentation, 20^{th} to 23^{rd} of February 2017, CERN, Switzerland

4. J.M.C. Perdigoto *et al*, " DCE 2017 - Symposium on Engineering Physics - Influence of Additive Gases on the Ion Transport Properties in Xenon, oral presentation, 8^{th} to 9^{th} of June 2017, Oporto, Portugal

Poster Communications

5. J.M.C. Perdigoto *et al*, "Measurement of ion mobility in relevant mixtures used in gas detectors", poster communication, Avaliação Intercalar, 24^{th} of February 2017, University of Coimbra, Portugal

Contents

List of Figures

List of Tables

Nomenclature

α	**N**eutral **P**olarisability (Å^3)
μ	**I**on-neutral **R**educed **M**ass (u)
ALICE	**A** **L**arge **I**on **C**ollider **E**xperiment
Ar	**A**rgon
CBM	**C**ompressed **B**aryonic **M**atter
C_2H_6	**E**thane
CF_4	**T**etrafluoromethane
CH_4	**M**ethane
CO_2	**C**arbon **D**ioxide
CsI	**C**esium **I**odide
E	**E**lectric **F**ield (SI units- V/m)
E/N	**R**educed **E**lectric **F**ield- expressed in Td (1 Td = 10^{-21} V/m^2)
GEM	**G**as **E**lectron **M**ultiplier
IDC	**I**on **D**rift **C**hamber
IE	**I**onization **E**nergy
k	**R**ate **C**onstant
K	**M**obility (expressed in $\mathrm{cm^2\,V^{-1}\,s^{-1}}$)
K_0	**R**educed **M**obility (expressed in $\mathrm{cm^2\,V^{-1}\,s^{-1}}$)
M	**N**eutrals **M**ass (u)
MWPC	**M**ulti **W**ire **P**roportional **C**hamber
m	**I**ons **M**ass (u)
N	**G**as **N**umber **D**ensity
N_0	**L**oschimdt **N**umber - 2.6867x10^{25} m^{-3}
N_2	**N**itrogen
QE	**Q**uantum **E**fficiency
R	**R**eaction **R**ate
Torr	unit of pressure based on an absolute scale. 1 Torr = 1/760 atm $\approx$ 133.3 Pa
TPC	**T**ime **P**rojection **C**hamber
TRD	**T**ransition **R**adiation **D**etector
UV	**U**ltra **V**iolet

$\nu_{\mathbf{d}}$	**D**rift **V**elocity (SI units- m/s)
Xe	**X**enon

Chapter 1

Introduction

1.1 Objective and Motivation

This Master thesis intends to expose the work done on the field of ionic mobility, more precisely in the study of gaseous mixtures based in Xenon, being this study associated with the need to collect reliable data on ion transport properties of relevant mixtures for the ALICE TPC. Futhermore, with the data collected it will be possible to conduct a study on the rate capability of Multi-Wire Proportional Chambers (MWPC's).

Although the data on ion mobility for mixtures of two gases is scarce, such knowledge is of great importance for the performance of large volume gaseous detectors, like the ALICE TPC. In fact, the build-up of positive space-charge in the large volume detectors (approximately 90 m^3 drift volume of the upgraded ALICE TPC) determines the feasibility of a sufficient on-line correction of the track distortions for immediate data compression, which of course influences the signal formation of the detector.

In the case of the MWPC, the data collected on ion mobility also affects deeply the performance of this detector. Typically, this instrument is employed in experiments needing high resolution tracking, like the ALICE TRD and CBM TRD. That being said, the measurements obtained for the ionic mobility on gaseous mixtures will be addressed on chapter 4.

1.2 State of the Art

The initial studies conducted on ion mobility and the progress on early analytical devices took place between late 19^{th} century and throughout the first three decades of the 20^{th} century. This revolution period is the result of studies performed by research centers in England and Germany where the phenomenon of electrical discharges in air and other

gases at atmospheric pressure was seen, leading to the conclusion that gases could transfer charge from insulators to conductors of electric current using several methods.

From this studies, it was stated that the conductivity in the gas was due to the formation of eletrons and ions, resulting in new researches to identify and determine the mobility of these ions. This lead, for example, to experimental studies on ion mobility using X-ray sources, started by Rutherford [1].

In order to understand the nature of this phenomenon, a theoretical study on ion mobility was published, in 1905, where it is depicted the importance of attractive forces of a charged particle on a neutral molecule and its effect on the mobility of ions in gases [2]. This approach, grounded on the polarisation interaction, was studied theoretically by Paul Langevin and lead to a comprehension of the results on the studies conducted in experimental ion mobility at atmospheric pressures.

Later on, in 1918, Chapman and Enskog developed a more general theory, that was applied to the calculation of mobilities and diffusion coefficients. Neverthless, both theories are constrained to spherically ion-molecule combinations and to small E/N [3].

After these studies, in 1916 and 1918, Max Trauz and William Lewis, independently, proposed a collision theory that explains how chemical reactions arise and why reaction rates vary for different reactions. This theory is related with the kinetic theory of gases and is valuable to predict which chemical species will be originated in some experimental systems that do not have a mass spectrometer, for example [4].

Prior to 1930, few reliable experimental techniques were available to measure the transport properties of ions in gases under the influence of an eletric field. A major drawback, in the results obtained at that time, were impurities, which had a significant role in the gas samples handled and, of course, conducted to some contradiction in the results of experimental mobility values. Solving those problems allowed the implementation of changes, such as improvements in gas handling techniques and construction of new methods for measuring mobilities, which lead to more reliable and reproducible data [3].

By the end of the 30's decade, Tyndall and his partners from Bristol University made a huge breakthrough in the study of experimental ionic drift velocities [5]. This was accomplished after important measurements of mobilities by constructing the four-gauze electrical shutter method. In Loeb [6], it is said that this method was one of the most reliable ones and it was quite used, with some important features at his disposal like high resolving power that yielded mobility values with great accuracy, allowing the study of pure gases well below the atmospheric pressure.

Twenty four years after Tyndall's experiment, this work was replicated by Beaty, with the purpose of improving the results taken previously, taking advantage on the

advances in electronics and vacuum techniques. None of these apparatus employed a mass spectrometer, neverthless both systems produced results capable of being easily analysed and interpreted [3].

A slow development up to the early 1950's was seen in the transport theory for ions in gases, until Wannier published, in 1953, a theoretical paper on the issue of the motion of ions in gases in the presence of strong electric fields. As reported by the author, for high *E/N*, the motion is assumed to be characterized by a constant mean free time and in this case the total energy of the ion consists on three parts, namely, thermal energy, drift energy and random field energy [3, 7].

In the early 60's, the development of the drift tube mass spectrometer showed an important step forward on the measurement of mobility and mass identification of ions in certain mixtures, enlightening the complicated effects of chemical reactions between the ions and gas molecules. By the later 60's, reliable data on ionic mobilities, and for the first time, on diffusion coefficients, appeared for several gases and ionic species [3].

Consequently, a major compilation of experimental data on ionic mobilities and diffusion coefficients for ions in neutral gases under an external applied electric field at room temperature was performed by H.W. Ellis, R.Y. Pai, E.W. McDaniel, L.A. Viehland, E.A. Mason, M.G. Thakston, D.L. Albritton and S.L. Lin. This compilation gathers four parts, with the first published in 1976 and the last one made being a literature coverage of the experimental data up to 1995 [8–11]. Some of the data presented in these papers was used in chapter 4.

1.2.1 Ion mobility spectrometers and commercial applications

Following the development of the drift tube mass spectrometer, the ion characterization at atmospheric pressure, grounded on the knowledge acquired on ion-molecule interactions, led to a development of an analytical technique, the Ion Mobility Spectrometry (IMS). This technique was used to identify elements by drift velocity of their ions in gas-phase under a weak uniform electric field, enabling the detection and identification of volatile and semi-volatile organic compounds [1].

The first ion mobility spectrometers was available commercially in 1970 for military and security purposes. At the same time, there were efforts to conceive intruments for detection of explosive and drugs, these being the main areas of commercial study. However, with the advances in technology, the new IMS spectrometers could improve their performance, in terms of detection sensitivity, response time, and also in portability, enabling their usage on a wide diversity of areas, namely food analysis, space exploration, biological applications, clinical analysis, medical purposes, petrochemical and environment analysis [12].

FIGURE 1.1: Commercial ion mobility spectrometer

The most common compounds usually detected are amido derivates which show high proton affinity in drugs, nitro groups due to its high electronegativity in the presence of explosives and halogen atoms stressing out high electronegativity or organophosphorous groups with high proton affinity in chemical warfare agents [1].

Example of portability and aplicability of this technology is the MMTD as shown in figure 1.1. The MMTD is a portable detector that can trace explosives, narcotics, toxic industrial chemicals (TIC) and chemical warfare agents (CWA). It can detect more than 50 hazardous substances (including ammonium nitrate used in home-made explosives) in approximately 10 seconds.

1.3 Contribution

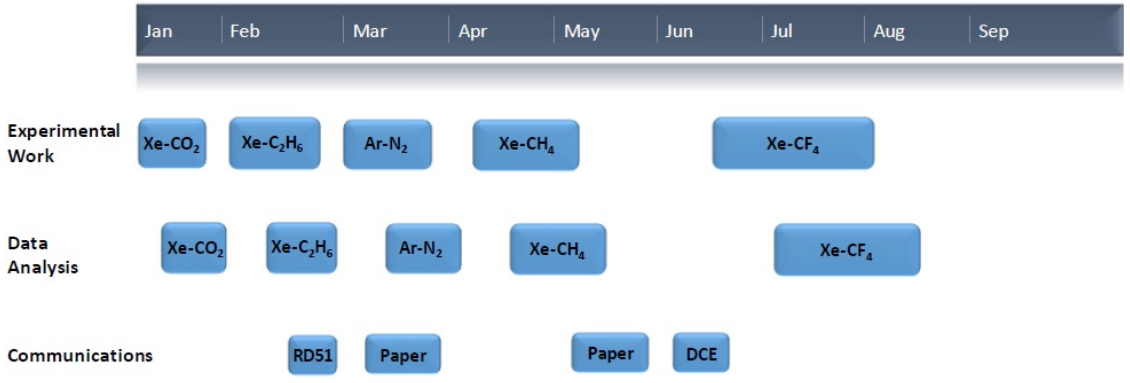

FIGURE 1.2: Timeline regarding my contribution since I joined LIP-Coimbra

Since the development of the experimental setup by Pedro N.B. Neves [4], different studies of ion mobility were accomplished [13–29]. Since I joined this group,

four different studies of ion mobility in mixtures were performed. All of the results in this work were obtained at room temperature, pressure of 8 Torr and for reduced electric fields (E/N) between 10 - 25 Td. A detailed timeline of the work accomplished can be found in fig. 1.2.

So, during the work conducted in the aim of this MSc thesis, I performed measurements in:

- **Mixtures of Xe-C_2H_6**
- **Mixtures of Ar-N_2**
- **Mixtures of Xe-CH_4**

The results and analysis of these measurements are presented in chapter 4 and in the appendix A of this report.

Chapter 2

Ion Transport Processes in Gases

2.1 Ionization mechanisms and ions formation

The ion source in mobility setups has the job to perform the task of creating the ions that will drift in the gas. A wide range of ionization methods can be used, being the most common the procedure of ionization involving electron impact on a neutral gas (A).

In fact, if an energetic electron with a kinetic energy of several tens of electron-volts (eV) collides with a neutral atom/molecule, some of the energy is transferred to the neutral. Although only part of the collisions are effective, in the ones which are, the energy transferred by the electron can exceed the ionization energy (IE) of the neutral (A), that corresponds to the minimum amount of energy that needs to be absorved by a neutral to originate an ion. This process can be represented by:

$$A + \mathrm{e}^- \longrightarrow A^+ + 2\,\mathrm{e}^- \tag{2.1}$$

and usually, the electron ionization predominantly creates singly charged ions from the neutral.

This ion will then drift in the gas, colliding with the gas molecules, eventually originating more complex secondary ions. In the context of this work, some mechanisms have a special relevance and they will be briefly described.

The charge transfer reaction corresponds to an interaction between an ion and a neutral, which might be a molecule or an atom. If the energy gained by the cation exceeds the energy necessary to remove an electron from the neutral, i.e. exceeds the ionisation energy, then the process of charge transfer can occur. Considering, the ion (A^+) and the neutral (B), the charge transfer is translated by:

$$A^+ + B \longrightarrow A + B^+ \tag{2.2}$$

If A and B are identical atoms, it is often known as resonant charge transfer:

$$A^+ + A \longrightarrow A + A^+ \tag{2.3}$$

Normally, these reactions have a significant impact in the drift velocity of the ion, since a delay can occur. Also, these reactions tend to be correlated to the discrepances of the mobility of a detected ion and the predicted value given by the limit predicted by the Langevin theory (eq. 2.15). One case in which this change of values occurs corresponds to CO_2 gas and its mixtures.

Another mechanism is cluster formation. Cluster ions are composed by a central ion with one or more neutral atoms and molecules attached to it. They bind together by the attractive force between the ion charge and the charge induced on the molecules. Typically the binding energy between them is in the 0.1 – 1.5 eV range, between that of chemically bound molecules and the van der Waals ones [22]. Considering the simplest cluster, with only one neutral, being as the same species of the ion, it is described by the reaction 2.4.

$$A^+ + A + M \longrightarrow A.A^+ + M \tag{2.4}$$

The element M is a neutral (A or B or, in some cases an impurity).

2.2 Reaction Rate

The collision theory, proposed by Max Trauz and William Lewis in 1916 and 1918, is based on the notion that reactant particles must collide for a reaction to take place. Nonethless, only a part of the total collisions have the required impact energy and the right orientation of the reactants, so that, at the moment of the impact they actually react and transform into products. These are called effective collisions.

Supposing a chemical reaction between two different species, A and B, originating products C and D:

$$aA + bB \longrightarrow cC + dD \tag{2.5}$$

where a, b, c and d consist on the stoichiometric coefficients. The speed at which this reaction develops is related with the reaction rate R, which is directly proportional to the

change in the concentration of a chemical species involved in the reaction as a function of time. Rising the concentration of the reactants or increasing the temperature results in the occurance of more successful collisions increasing the rate reaction, given by:

$$R = -\frac{1}{a}\frac{\mathrm{d}[A]}{\mathrm{dt}} = -\frac{1}{b}\frac{\mathrm{d}[B]}{\mathrm{dt}} = \frac{1}{c}\frac{\mathrm{d}[C]}{\mathrm{dt}} = -\frac{1}{d}\frac{\mathrm{d}[D]}{\mathrm{dt}} \tag{2.6}$$

where $[A]$, $[B]$, $[C]$ and $[D]$ represent the concentrations of the species. In most cases, R can also be expressed by :

$$R{=}k[A]^m[B]^n \tag{2.7}$$

where k is the rate constant, while the sum of m and n represent the order of reaction regarding A and B. Important to note that the reaction order does not always correspond to the stoichiometry of the reactant, except in elementary reactions, like in the case of first-order reactions ($A \longrightarrow$ products), where the reaction rate is expressed by:

$$R = k[A] = -\frac{\mathrm{d}[A]}{\mathrm{dt}} \tag{2.8}$$

Integrating eq. 2.8 in order of time, an expression of $[A]$ is attained.

$$[A]_t{=}\,[A]_0 \cdot \mathrm{e}^{-kt} \tag{2.9}$$

being $[A]_t$ the concentration of reactant A after a period of time t and $[A]_0$ corresponds to its initial concentration.

However, in our experimental system it is more likely that bimolecular reactions occur. The reaction rates with respect to the second chemical reaction order are given by (with m=1 and n=1):

$$R = k[A][B] = -\frac{\mathrm{d}[A]}{\mathrm{dt}} \tag{2.10}$$

The same deduction can be made for these reactions, although with an increase in the reaction order, the differential equation becomes more complex to solve and to track the true concentration concentration of the different reactions. As a way to found a solution, it is used the pseudo-first-order method as an approximation. Considering the case of the second order reaction, if $[A] \gg [B]$ the concentration of A is assumed to remain constant during the reaction, and eq. 2.10 can be deduced as:

$$\frac{\mathrm{d}[A]}{\mathrm{dt}} = -k_{(2n)}[A][B] = -k_{(\mathrm{n})}[B] \tag{2.11}$$

where

$$k_{(\mathrm{n})} = k_{(2n)}[A] \tag{2.12}$$

and the index n, $2n$ respects to the reaction order. The units of the reaction constant depends on the reaction type.

In chapter 4, this method is used as an approximation to solve the differential equations in order to plot the concentration of the ions versus the reaction time.

2.3 Transport properties of Ions in gases

2.3.1 Drift and Mobility

If a weak, uniform electric field is applied to the group of ions then these ions will gain energy from the electric field, but may also lose energy by collisions with the neutral molecules of the gas. Taking these factors into account, a steady state can be reached and under these circumstances the resulting average speed of this group of ions, also known as drift velocity, ν_d, is directly proportional to the electric field intensity, E, given the following expression:

$$\nu_d = KE \tag{2.13}$$

where K is the mobility of the ions. This expression is valid for low electric fields (below 30 Td),when the energy gained by the ions from the electric field is lower than by thermal energy. In the literature, the ion mobility, K, is often address in terms of reduced mobility, K_0, given by

$$K_0 = KN/N_0 \tag{2.14}$$

being N the gas number density and N_0 the Loschmidt number ($N_0 = 2.6867$ x$10^{25}\,\mathrm{m}^{-3}$).

2.3.2 Langevin's Theory

In the Langevin's theory [2], three assumptions are made. First, both ions and atom-s/molecules of the gas act like hard spheres, being the ato-ms/molecules polarisable in the field of the ions. Second, the interactions between atoms and ion only have two origins: the polarisation attraction and the hard sphere repulsion. Finally, the velocity distribution of ions and molecules is considered a Maxwell-Boltzmann distribution.

The Langevin limit for the ion mobility corresponds to the value of K_0 in the double limit of low E/N and low temperature, conditions which ensure the dominance of the polarization attraction over the hard sphere repulsion. This limit is given by eq. 2.15,

$$K_{\text{pol}} = 13.88\,(\frac{1}{\alpha\mu})^{\frac{1}{2}} \tag{2.15}$$

where α is the neutral polarisability in cubic angstroms (α = 4.044 Å^3 for Xe [30], α = 4.47 Å^3 for C_2H_6 [3] and α = 2.62 Å^3 for CH_4 [31] and μ is the ion-neutral reduced mass (u), described by equation 2.16, wherein M and m are the neutral and ion' mass, respectively.

$$\mu = \frac{mM}{m+M} \tag{2.16}$$

The Langevin limit can be obtained from the low-field expression for K assuming that the polarisation is the predominant interaction taking part in the ion-neutral collisions. The deduction of this expression can be found in [4].

An aspect to be considered is that if the polarisation attraction is already dominant at room temperature, a limiting value for the mobility at room temperature is also expected. A decrease in the temperature only increases the predominance of the polarisation interaction, though not significantly [32].

Usually, eq. 2.15 gives values of ionic mobilities that are in good agreement with experimental observations at room temperature [15, 17]. However, there are some deviations from the Langevin limit that are usually attributed to chemical reactions with impurities or the presence of charge transfer processes, defined in section 2.1.1.

The Langevin limit does not have a way to account for the impurities and the charge transfer processes, since it is difficult to incorporate these effects in the formula. However, concerning the cluster formation, in the Xe-CO_2 mixture a new method was considered as a way to predict the theoretical mobilities values of $CO_2{}^+ \cdot CO_2$ [22].

Another limitation besides the ones mentioned above, concernes the applicability of the Langevin limit. For this conditions to take place the value of K_0 corresponds to the double value of low E/N and low temperature. Nevertheless, since our experimental conditions report to reduced electric fields between 10 Td and 25 Td at ambient temperature, the Langevin limit is respected.

2.3.3 Blanc's Law

The Blanc's empirical law has proven to be useful when determininng ions mobilities using mixtures of gases, as seen from previous work done by Blanc in the mobility of ions in binary gaseous mixtures. This way, Blanc found that the mobility of ions in gaseous mixtures, K_0, followed a relation in most cases. Exceptions can happen if charge transfer interaction is not negligible compared to the polarization attraction and short-range repulsion between ions and atoms/molecules.

This relationship can be expressed as follows:

$$\frac{1}{\mathrm{K_{0mix}}} = \frac{\mathrm{f_1}}{\mathrm{K_{0g1}}} + \frac{\mathrm{f_2}}{\mathrm{K_{0g2}}} \tag{2.17}$$

where K_{0mix} is the reduced mobility of the ion in the binary mixture; K_{0g1} and K_{0g2} the reduced mobility of that same ion in an atmosphere of 100% of gas 1 and gas 2 respectively; f_1 and f_2 are the molar fraction of each gas in the binary mixture [33].

The use of the Blanc's Law as a cross-check method to determine which ions were formed in our experimental setup by comparing the reduced mobility experimental values with the theoretical values has proven to be very useful at all the experiments performed.

However, in some cases, this method may not be as useful as it should be, given that Blanc's law does not take into account effects like the presence of impurities, charge transfer processes or the formation of clusters. All these effects tend to slower down the ions formed, therefore the reduced mobility values obtained experimentally wil differ from the ones predicted by Blanc's law.

Chapter 3

Methods and Experimental Setup

After some theoretical considerations, it becomes relevant to describe the experimental system used to perform these studies of positive ion mobility measurements in gas mixtures.

This experimental system has proven to be a valid instrument in the measurement of ion mobility, providing the ion identification in gases of interest, as confirmed by the several scientific contributions.

In section 3.1 the experimental setup will be described, focusing on the components of the detector, on how the vacuum was performed in the system, addressing the issue around the gas filling and gas purity.

In section 3.2, the ion identification process will be discussed, while in section 3.3 some limitations of this system will be referred too.

3.1 Experimental Setup

The experimental setup used to perform the measurements is depicted in figure 3.1.

In fact, some important parameters can be highlighted in this system, like the ion drift chamber and the pre-amplifier developed for the detection of cations and the amplification of the charge signal. Also, it is ilustrated the pressure gauges used which have the function of controlling the pressure of the mixture studied or to verify if there is a proper vacuum level to start the gas filling. The detected signals are recorded in a digital oscilloscope, before being fed to a PC for analysis.

The system is based on the final prototype that was built by P.N.B Neves between 2005 and 2009 [4].

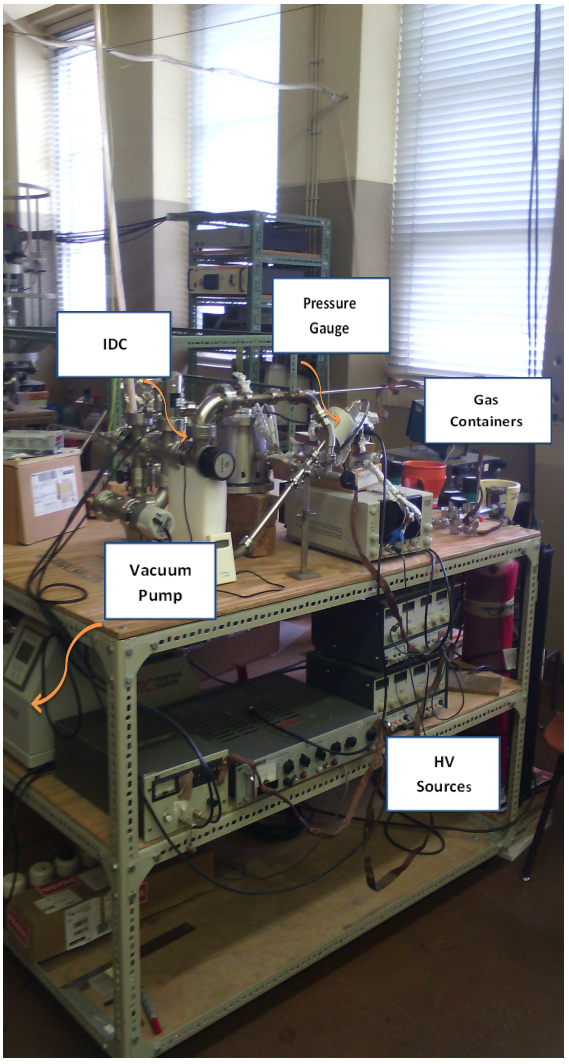

FIGURE 3.1: Experimental Setup

3.1.1 Operation Principle

A schematic of the Ion Drift Chamber (IDC) and of its working principle is depicted in figure 3.2. The measurements start with a flash emitted by the Hamamatsu Xenon Flash UV lamp, which emits photons at 10 Hz frequency and a pulse duration shorter than 0.5 μs. Upon their release, the photons will reach the CsI photocathode coated on the top of the Gaseous Electron Multiplier (GEM), thus releasing photoelectrons.

Due to the GEM's polarisation, the released photoelectrons are guided through its holes, all the way to the GEM's bottom. While taking this path, they gain energy due to the potential difference established, allowing the ionization of gas atoms or molecules when the electrons' energy surprasses the gas ionisation threshold. As a result from this process, the electrons start to multiply in avalanche, increasing largely throughout the

holes [4], process explained by the energy that the electrons gain through their path, which is almost similar to the potential difference between top and bottom of the GEM. The effects of controlling the energy of the electrons, are address with more detail in section 3.2.

So, the electrons are conducted to the bottom electrode of the GEM, where they are collected, while the positive ions that result from the ionization of the gas molecules in the GEM holes drift across the drift region towards grids G2 and G1 under an uniform electric field. Throughout the drift distance the uniformity of the electric field is reassured by the stainless steel discs along the way. Grid G2 acts as a Frisch grid to prevent signal induction in G1 by the positive ions while they travel through the drift region. Therefore, the signal induced by the ions in G1 concerns only to the portion of the cation's motion between G1 and G2.

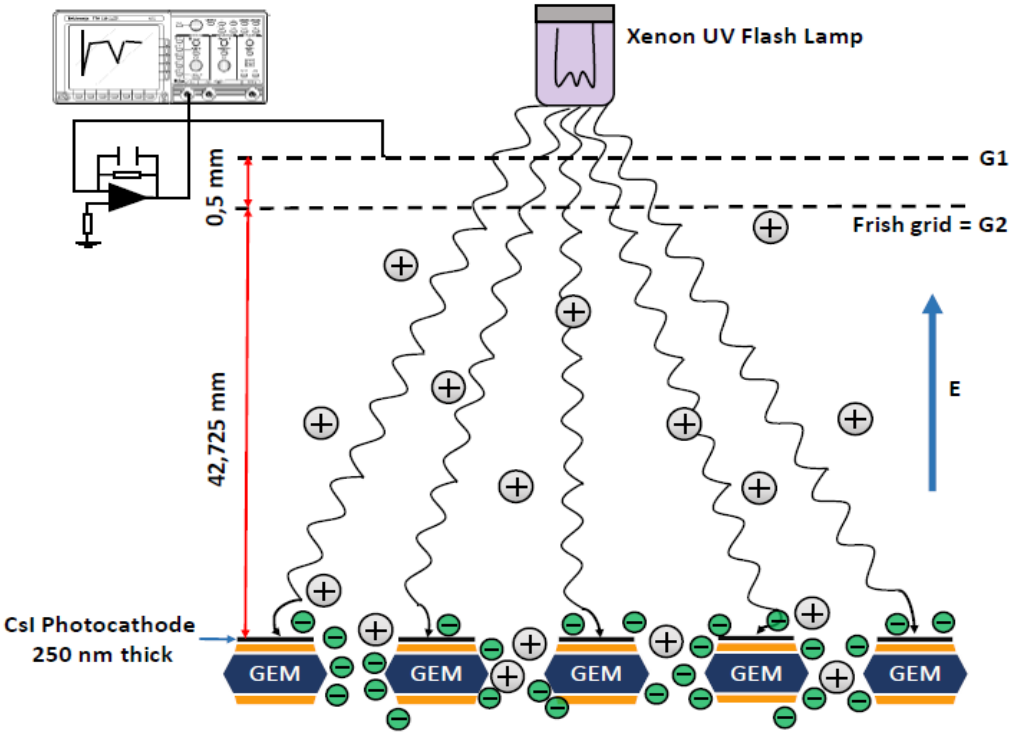

FIGURE 3.2: Schematic diagram of the production and detection of ions. Scheme taken from [35].

As shown in the figure 3.2, the electrical pulse collected in the grid G1 is now converted from current to voltage, with a pre-amplifier allowing to obtain a time of arrival spectrum in a digital oscilloscope (Tektronix TDS 1012). In order to account for flutuations on the recorded pulse, an average of 128 pulses is performed. This recorded

signal is then fed to a computer for a posterior processing with a specially developed code in Matlab.

By fitting the spectra with gaussian functions, we are able to retrieve the information on the peak centroid which corresponds to the average drift time of the group of ions. Knowing the drift distance, the velocity can be calculated, and knowing E and using eq. 2.13, the mobility is found.

This IDC is connected to the gas system through two gas inlets from where the gases flow when admitted or released, before and after the measurements were done, respectively.

Concerning the electric field uniformity, it was achieved by attaining several 2 mm thick stainless steel rings equally spaced using Teflon spacers. A correct voltage was set to the rings using a resistor chain of 2.76 MΩ.

In the last disk of stainless steel is incorporated the GEM, where the ions are originated.

The GEM's thickness is 60 μm, with 50 μm of Kapton and a 5 μm copper layer on each side. It has an active area of 10x10 mm^2 and it was assembled on a G-10 (glass fibre material). The GEM holes have a wider diameter of 70 μm at the metal surface and a inner diameter of 55 μm in the insulating layer. These holes have an hexagonal spatial arrangement wherein the center of each hole is distanced 140 μm from the others [34].

Due to the geometry of the GEM, namely to its thickness, the drift distance travelled by the cations is known with great accuracy, since these cations are formed mainly in the GEM holes, with a thickness very small (order of hundreds of μm) compared to the drift distance (order of few cm).

As already mentioned, the ionization of the gas molecules is achieved through the electric field that is applied between the two electrodes of the GEM, using two high power DC supplies, Fluke 415B and HP 6110A. The first one is coupled to the top electrode of the GEM, which is used to establish the electric field in the drift region of the chamber, while the second one is coupled to the bottom electrode. The voltage difference between these two electrodes limits the maximum energy gained by the electrons.

A 320 nm thick layer of high purity CsI vacuum deposited on the top surface of the GEM acts as a photocathode, thus initiating the process of ion production.

As already mentioned above, the cations are detected and collected in a double grid which corresponds to two meshes, commonly adressed by G1 and G2, separated by a 0.5 ± 0.1 mm thick MACOR spacer. The meshes are of stainless stell wire, 80 μm in diameter and 900 μm in spacing. The voltage difference between these grids was set at 30 V by a precision DC power supply, Thandar TS2022S.

A DC power supply Topward 6303D feeds the Hamamatsu Xenon UV Flash Lamp (model L2439) which operates at a repetition rate of 10 Hz and with the a pulse width (FWHM) inferior to 500 ns.

Concerning the question of the collection of cations by grid G1, a voltage pre-amplifier is used with the intention of amplificating of the pulses received. It is a high density charge sensitive pre-amplifier, model A250F/NF, designed by AmpTEK. The electronic coupling of the amplifier was chosen to maximize the gain of the signal, while reducing the electronic noise [4]. The pre-amplifier was shielded with a copper box, in order to avoid the electronic noise from external sources. Such device is connected to an oscilloscope, where the signal is read and analysed.

3.1.2 Gas Handling System

The gas handling system where the IDC is placed, ilustrated schematically in fig. 3.3, includes a gas admission system and an evacuation system.

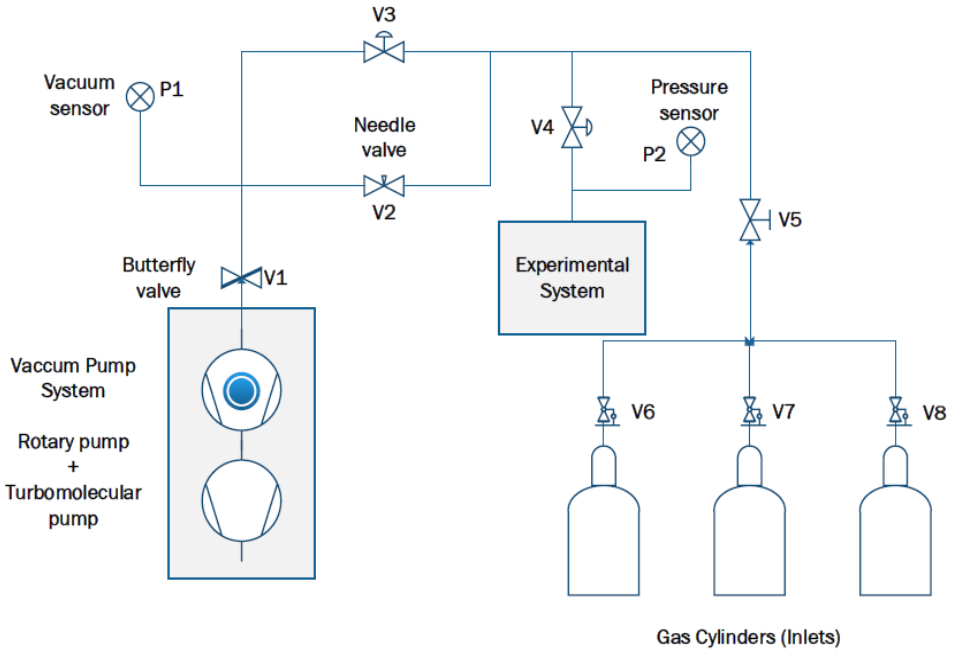

FIGURE 3.3: Schematic of the vacuum system used to evacuate the experimental system [35] and then fill with gas from the gas containers. **P1** and **P2** are the pressure sensor that measures the pressure of the vacuum system during the evacuation and pressure of gas inside the detector, respectively. *Vi*, i=1,2,...,8 are the valves used in the vacuum system.

The vacuum is made using an Edwards EXPT Pumping Station. This pumping system has a fully automatic pumping system composed by a backing pump that performes vacuum at a medium-level vacuum, up to 1.5 Torr, and a turbomolecular pump which can evacuate down to 1x10 $^{-7}$ Torr [36].

To obtain a proper vacuum in the complete system, it requires the opening of valves V1, V3, V4 and V5, allowing the removal of gas from the system.

The vacuum quality in the system is assessed with a vacuum sensor, an Edwards WRG-S-NW25, expressed as P1 in the scheme above. It consists in a gauge combination that relies on Pirani technology for the upper pressure range from atmospheric pressure to 3.7x10^{-4} Torr, with a uniform switch that changes to an inverted magnetron for the lower pressures. This offers the capability of a single port for the pressure measurement in the range from atmospheric pressure to 7.5x10^{-10} Torr with a linear output, which makes its use suitable for our experimental conditions [37].

As far as the valve *V1* is concerned, when the vaccum pump system is turned off, it gives a direct isolation of the vacuum line from the ambient pressure, given the air admittance in the vacuum system, while it is shut off. Meanwhile, the valve *V4* enables the isolation of the detector from the experimental system, preventing some leak to damage the detector or only to apply vacuum in the rest of the system. Looking to scheme, the *V5* valve acts as a way to isolate the region of gas admission from the whole system, when a gas cylinder container or more needs to be switched.

When we speak of gas' admission in the system, there are three inlets, with the possibility of installing three gas cylinders The gas' admission of the system is accomplished through the gas cylinders installed in the three inlets at our disposal, making the proper mixtures for the experiment. The process to introduce the right amount of each gas in detector, requires some precision, so the pressure of gas introduced is verified by a digital display Edwards 1575 MON ANALOG connected to a membrane pressure gauge Edwards Barocel Pressure Sensor 600AB Trans 1000TR [38], named P2 in the scheme. Also, for the admission process, the valve V3 must be closed.

Filling Process

Even with the admission procedure already presented, the process of filling requires some caution, mainly in the case of admixtures or when the gas stays inside the detector more than it should be, due to impurities from outgassing process. In these particular cases, the best option is to vacuum up all the gas inside of the detector and perform the same measurement again.

Also, the order in which the gas is added in the detector affects the error in

the composition of the desired mixture, given that the pressure gauge (P2) has a reading accuracy of 0.15 %. As the error is directly proportional to the pressure, the gas with a lower percentage in the mixture, this is with lower partial pressure, should be added first, reducing the overall error of the pressure.

The experimental studies documented in this paper were done using different high purity gases. The datasheet of the purity of the gases is indicated by the manufacturers [39–44]. Since our experimental system does not have gas purification, this data is quite important.

3.2 Ion Identification Process

As seen from our experimental setup, we do not possess any mass spectrometer that permits the direct identification of ions, neverthless this system offers some features allowing an alternative way of identification. So, we will describe in general this approach.

The most relevant feature of this method is the capability of setting the voltage across the GEM (V_{GEM}), which is related with the energy attained by the photoelectrons as they drift along the GEM holes. According to the voltage value applied and knowing the ionization energy of the primary ions of the gas, we can identify these ions. After this identification, it's possible to point out the secondary reaction paths, identifying the main candidate ions.

Blanc's law can then be used to help in the identification of the ions present in different mixtures. Through the comparision of mobility values obtained experimentally using the expression 2.13 that correlates the drift velocity with the reduced electric field and those calculated with Blanc's law. This corresponds to our method of cross-checking to identify the final ions in the mixture.

In order to validate this elaborated method described, it is important to take into account the significance of knowing the dissociative channels, product distributions and rate constants that assume a major role in identifying the best suited ion candidates responsible for the peaks shown in the spectra. This will be addressed in more detail in chapter 4, where we present the results.

3.3 Limitations to the Experimental Measurements

In order to operate this device, it becomes relevant the understanding of its limitations, since its incorrect use may lead to misinterpretation of the collected data. Inherent limitations to our experimental system include the effect of impurities caused by the system

outgassing, the limits on the reduced electric field values and on pressure values that allow to obtain a reasonable induced signal by the group of ions in the grid without electric discharges that could damage the components. Finally, there are also some limitations due to the electronic equipment used.

Gas mixtures with a large level of water should be avoided as well as the CsI film used is highly hygroscopic and this would lead to the deterioration of the signal amplitude (highly dependent on the quantum efficiency of the photocathode used).

The impurities previously spoken tend to efficently convert the ions normally observed in the studied gases, particularly Ar, in other types of ions through collisions. Considering impurities when these are polar or highly polarisable, they tend to produce clusters or they can be ionised by the primary ions through charge transfer processes. In P.N.B. Neves [4] a study was performe on the influence of impurities in the induced signal for rare gases. These impurities may be due with two origins, these being outgassing problems and prevailing impurities in the gases used. Outgassing is due to the slow release of gases that were trapped, frozen or adsorbed in the chamber material. The overall impact depends substantively on the materials used which have different rates of outgassing related with the contact area of the material and the volume detector. Furthermore, the rate of outgassing has a dependance with temperature, so the majority of impurities within this particular system is water vapour since we operature at ambient temperature [45]. It is possible to reduce the outgassing using a vacuum pump along and by heating the experimental setup, since heating the chamber would improve the system outgassing. Unfortunately, this last step is not possible because the epoxy used to glue the feedthroughts does not not withstand temperature above 100 °C. Finally, concerning the impurities in the gas, those are tabulated by the manufacturer.

Despite the inherent presence of impurities in our device, there still is a way to reduce its impact in our measurements starting with a rigorous gas filling procedure. In fact, all measurements were obtained in 2 - 3 minutes time interval to avoid the degradation of the ion's induced signal due to outgassing, however no measurement was considered until the spectra obtained stabilised. The vessel was evacuated before each measurement to pressures read in P1 of 10^{-6} - 10^{-7} Torr.

Considering the range of the reduced electric field that could be used, in the upper limit, are the electric discharges that tend to occur; in the lower limit for values of E/N below about 5 Td it often occurs a deterioration of the time-of-arrival spectra, due to diffusion of ions in the drift region.

Finally, a last limitation that was not addressed corresponds to the range of pressures. In fact, the values of pressure used in all our experiment fall in the domain of low pressures, with values between 6-10 Torr, so no pressure dependence and its limitation

was studied in this work.

Chapter 4

Results and Discussion

4.1 Introduction

In this chapter we present the results and discussion of the mobility studies conducted for Xe mixtures, namely in binary mixtures with C_2H_6 (4.3.1) and CH_4 (4.3.2). The results for $Ar-N_2$ mixtures are presented in appendix A.1, although a discussion for this gas is not presented in this report.

Considering the measurements made for the binary mixtures described above, it was important to ensure that the results obtained are reproducible and trustworthy in our experimental conditions, since each mobility measurement for different conditions of field and voltage across the GEM was repeated for at least 5 times, and the final result obtained is the arithmetic average of all the results at same conditions and the associated error is the standard deviation from these measurements.

In section 4.2, four different types of graphics will be shown. The first one corresponds to a time-of-arrival spectrum that was recorded using a digital oscilloscope and corresponds to an average of 128 pulses, after a subtraction of the background noise. To the collected data is performed a signal de-noise and a gaussian fit to the peaks obtained. The second refers to a plot of the inverse of reduced mobility versus the relative amount of xenon, since it is the common denominator among the binary mixtures studied in this chapter.

In some cases, the nature of the peak is not well known or there are impurities that tend to sway the mobility of the ions detected, so for those cases a signal degradation study is performed. This procedure consists in keeping the binary gas mixture in the detector for a period of time longer than usual and recording the signal in equally spaced time intervals. From this analysis, the time-of-arrival spectra should present a evolution in the peaks relative abundance in case they are affected by the presence of impurity

components. These impurities are often associated to the formation of clusters or water ions, resulted from the outgassing processes or even by the purity's gas.

Finally, the last plot type exhibits the reaction paths that occur in a specific gas, discriminating which ions had enough time to be produced. The concentration of reactants were obtained through the numeric integration of eq. (2.12), when the pseudo-first order reaction could be applied.

The behaviour of rare gases (Xe, Ar) was object of studied by P.N.B. Neves in this experimental system [4].

4.2 Test of the experimental system

Before starting with the measurements proposed in this work, as a way to assess the work learning goals and validate the experimental data, a study of a prior mixture was performed, Xe-CO_2.

As mentioned in a previous chapter, in order to perform measurements in ionic mobility, it is important to have previously a good vacuum, of the order of 10^{-7} Torr at P1 (fig. 3.3). This level of vacuum was only achieved after numberous gas fillings and evacuations.

In fig. 4.1 are displayed the time-of-arrival spectra obtained previously to this work (a) 50 % Xe and b) 95% Xe) as well as the ones obtained in the scope of this initial work at the same conditions (c) 50% Xe and d) 95% Xe). The data was obtained using a E/N of 15 Td, a pressure of 8 Torr, V_{GEM} of 20 V and at room temperature of 293 K.

Looking to the time-of-arrival spectra, one can say that the ones obtained for this initial test agree with the ones obtained previous to this work, although some minor differences can be atributted due to the presence of impurities (like the presence of an extra peak for the 50% spectrum) and to shielding problems (as seen from the noise level displayed in a) and b)).

This behaviour might be explained with the presence of some impurities, often related to H_2O, that at the time were still in the system, affecting the spectra recorded, leading to the formation of a new peak. The presence of impurities is known to decrease as well the mobility of ions at high pressures [22].

Regarding the 95% Xe-CO_2 the spectra show that apart from the electronic noise at base level, these two spectra are almost identical, meaning that the system was already displaying good results.

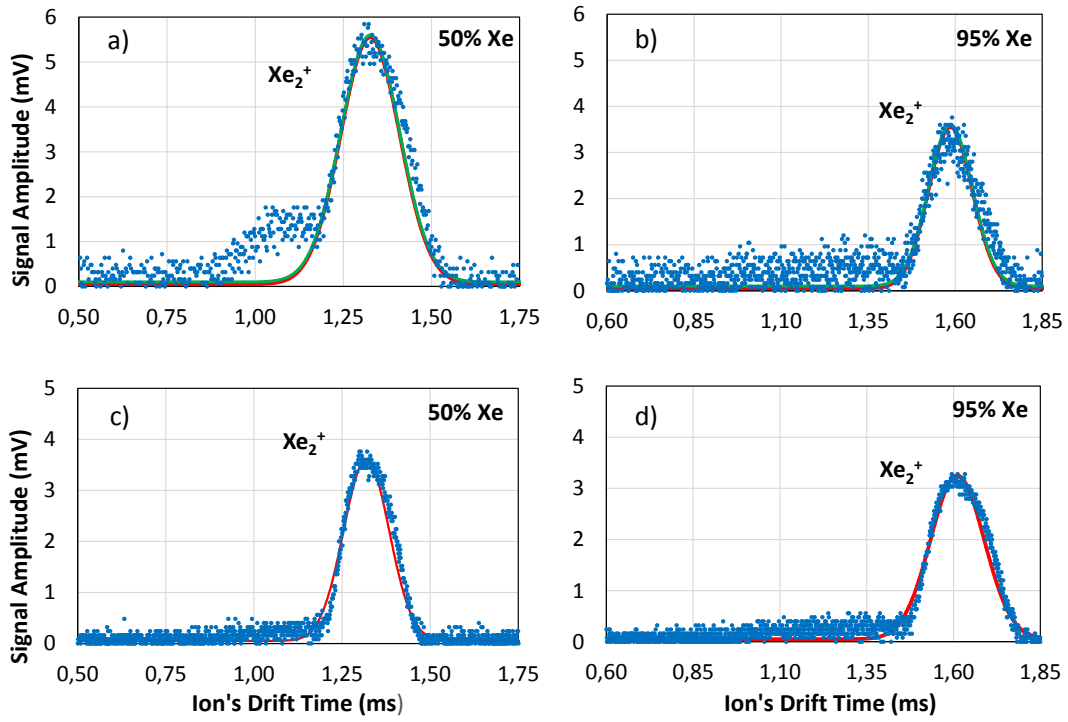

FIGURE 4.1: Time-of-arrival spectra for 50% and 95% of Xe in Xe-CO_2 mixtures, with a) and b) corresponding to this study while c) and d) corresponding to a prior study of this mixture [26].

After these measurements, the problems mentioned above were solved, namely the shielding and the extra peak, leading to spectra that resembled with the ones previous to this study.

According to [26], the ion responsible for the peak was found to depend on the mixture ratio, given the cross sections and rate constants, so for Xe concentrations down to 15% the ions are from Xe (Xe_2^+/Xe^+), while below this concentration the main ion is believed to be a CO_2 ion ($CO_2^+ \cdot CO_2$).

Once the time of arrival spectra for a wide range of concentrations of the mixture were recorded, it was plotted the inverse of reduced mobility obtained for the ions produced in Xe$-CO_2$ mixtures as a function of the percentage of Xe, for 8 Torr and 15 Td, at room temperature, as seen in fig. 4.2. Also in the same plot are projected the Blanc's law prediction for Xe_2^+ (blue dashed line), Xe^+ (green dashed line) and $CO_2^+ \cdot CO_2$ (orange dashed line), data from this study (border green square dots) and data from the previous study [26] (blue dots). K_{g1} and K_{g2} in Blanc's law (eq. 2.17), were obtained either using experimental values from literature or, when not possible, by using the Langevin limit formula (eq. 2.15).

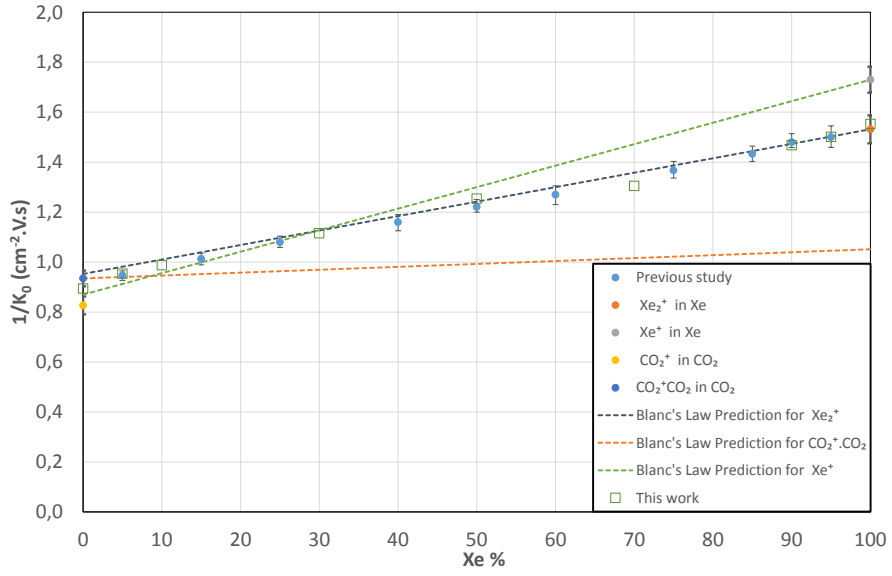

FIGURE 4.2: Inverse of the reduced mobility of the ions produced in Xe-CO_2 mixtures for a pressure of 8 Torr and for a E/N of 15 Td at room temperature.

As mentioned before, Langevin theory has some limitations, namely in CO_2, yielding mobilities higher than the experimental values. To address the lack of experimental values for Xe^+ and $Xe_2{}^+$ in pure CO_2 an alternative method was used with data from the work in [57] for pure CO_2.

Looking at fig.4.2, one can say that the ion mobility experimentally obtained follows Blanc's law prediction for the most abundant ion in the different Xe percentages studied, as expected [26].

Our analysis also included measurements taken within the range of reduced electric field of 10 - 25 Td at 8 Torr, where no significant variation of the mobility was observed. Table 4.1 summarizes the results obtained.

Taking into account this analysis and the study performed in [26], it is fair to acknowledge that our test analysis is in accordance with the majority of the range studied in [26], and for that reason we considered that the system was ready to start new measurements in other mixtures.

TABLE 4.1: Mobility of the ions observed for the Xe-CO_2 mixture ratios from pure CO_2 (0% Xe) to pure Xe (100 % Xe), obtained for different *E/N* and a pressure of 8 Torr at room temperature (293 K) and a voltage across the GEM of 20 V.

Mixture	15 Td	20 Td	25 Td	Ion
100% CO_2	1.12 ± 0.02	1.06 ± 0.02	1.05 ± 0.02	$\mathbf{CO_2 \cdot CO_2}^+$
5% Xe - 95% CO_2	1.05 ± 0.02	1.03 ± 0.02	1.03 ± 0.02	$\mathbf{CO_2 \cdot CO_2}^+$
10% Xe - 90% CO_2	1.01 ± 0.02	1.01 ± 0.02	1.00 ± 0.02	$\mathbf{CO_2 \cdot CO_2}^+$
30% Xe - 70% CO_2	0.90 ± 0.02	0.89 ± 0.02	0.88 ± 0.02	$\mathbf{Xe}^+$
50% Xe - 50% CO_2	0.80 ± 0.02	0.79 ± 0.02	0.79 ± 0.02	$\mathbf{Xe_2}^+$
70% Xe - 30% CO_2	0.77 ± 0.02	0.74 ± 0.02	0.74 ± 0.02	$\mathbf{Xe_2}^+$
90% Xe - 10% CO_2	0.68 ± 0.01	0.67 ± 0.01	0.67 ± 0.01	$\mathbf{Xe_2}^+$
95% Xe - 5% CO_2	0.67 ± 0.01	0.66 ± 0.01	0.65 ± 0.01	$\mathbf{Xe_2}^+$
100% Xe	0.64 ± 0.01	0.64 ± 0.01	0.64 ± 0.01	$\mathbf{Xe_2}^+$

4.3 Gas mixtures

4.3.1 Xe-C_2H_6

Using the method already described, a detailed study was conducted in xenon-ethane (Xe-C_2H_6) mixtures. The time of arrival spectra obtained already averaged for 128 pulses and with the background subtracted are shown in fig. 4.3. It is possible to see that in the range of mixtures studied, two main peaks were observed. These peaks were attributed to $C_3H_n{}^+$ (with higher mobility) and $C_4H_n{}^+$ (more intense). Meanwhile, for concentrations of Xe above 70% a bump starts to appear at the right side of the main peak for reduced electric fields higher than 20 Td, which was attributed to the resonant charge transfer of the $C_2H_6{}^+$ to C_2H_6. In the fig. 4.3 is shown the influence of the addition of Xe in the studied mixture.

TABLE 4.2: Ionization reactions, ionization cross sections for electron impact (at 20 eV) on Xe [49] and respective reaction rates.

Reaction	Rate Const.	Cross Sec.($10-1\,^6 cm^2$)	Ref.
$e^- + Xe \longrightarrow Xe^+ + 2\,e^-$	-	2.43	[49, 50]
$Xe^+ + Xe \longrightarrow Xe + Xe^+$	$2.5x10-1\,^0 cm^3 \cdot s^{-1}$	-	[51]
$Xe^+ + 2\,Xe \longrightarrow Xe_2{}^+ + Xe$	$2.0x10-3\,^1 cm^6 \cdot s^{-1}$	-	[52]

In this case, the total impact electron ionization cross section of Xe (table 4.2) ($2.43x10^{-16}$ cm^2) [49] is two times higher than that of C_2H_6 ($1.12x10^{-16}$ cm^2) [59] at 20

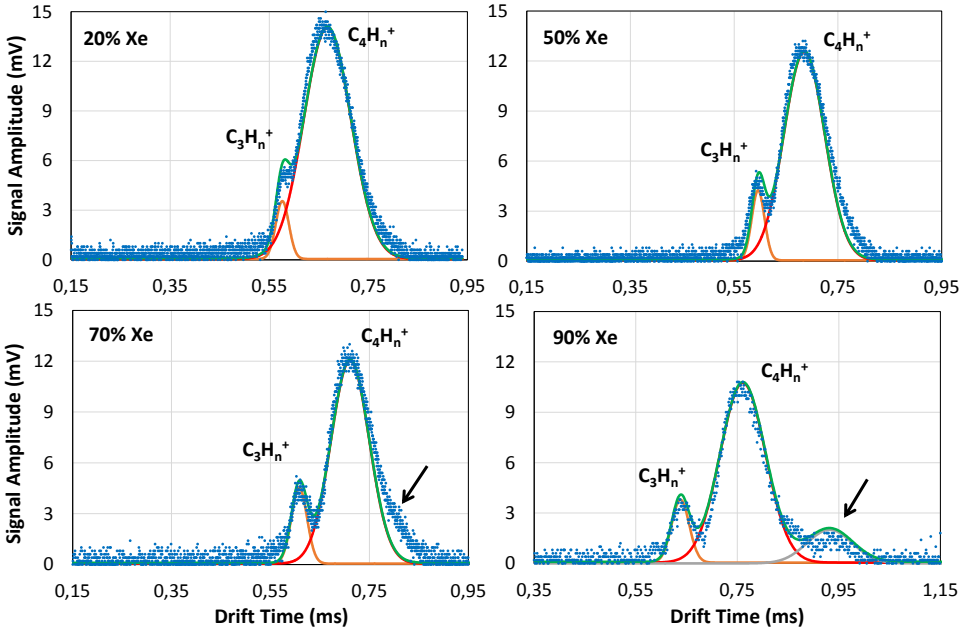

FIGURE 4.3: Time-of-arrival spectra of an average of 128 pulses recorded for several Xe-C_2H_6 mixtures (20%, 50%, 70% and 90% of Xe) at a pressure of 8 Torr, temperature of 293 K and for a reduced electric field of 20 Td with a voltage across the GEM of 20 V.

eV. So, it is then expected that even for low Xe concentrations (down to 30% Xe), Xe^+ ions are predominantly produced.

Nevertheless, these Xe^+ ions more rapidly undergo one of the possible reactions with C_2H_6 than with Xe, as shown by the rate constants in table 4.3 compared with table 4.2.

TABLE 4.3: Reactions involving Xe atomic ions and its ionization products with C_2H_6 [59, 60].

Reaction	Rate Const. (10^{-10} cm^3s^{-1})	Prod.Dist.	Ref.
$Xe^+ + C_2H_6 \longrightarrow {C_2H_6}^+ + Xe$	9.20 ± 1.84	0.55	[54]
$Xe^+ + C_2H_6 \longrightarrow {C_2H_5}^+ + H + Xe$	9.20 ± 1.84	0.10	[54]
$Xe^+ + C_2H_6 \longrightarrow {C_2H_4}^+ H_2 + Xe$	9.20 ± 1.84	0.35	[54]
${Xe_2}^+ + C_2H_6 \longrightarrow XeC_2{H_6}^+ + Xe$	6.80 ± 1.36	1.00	[61]

Therefore, these secondary reactions will lead to the formation of some of the primary ions found in pure C_2H_6 (${C_2H_6}^+$, ${C_2H_5}^+$, ${C_2H_4}^+$). In addition to this, for direct impact electron ionization of C_2H_6, the primary ions formed are the same, with few

exceptions to the previous ones (CH_3^+, $C_2H_2^+$, $C_2H_3^+$) (Table 4.4). In both cases these ions will rapidly undergo reactions with molecules of C_2H_6, which also transform them into secondary ions (table 4.5, resulting in the ones collected in the grid.

TABLE 4.4: Ionization reactions, ionization cross sections for electron impact (at 20 eV) on C_2H_6 [60], appearance energy (A.E) [59] and respective product distribution.

Reaction	Cross Sec. (10^{-16} cm^2)	A.E (eV)	Prod.Dist.
$e^- + C_2H_6 \longrightarrow C_2H_6^+ + 2\,e^-$	0.168	11.57	0.15
$e^- + C_2H_6 \longrightarrow C_2H_5^+ + H^- + e^-$	0.122	12.08	0.111
$e^- + C_2H_6 \longrightarrow C_2H_4^+ + H_2 + 2\,e^-$	0.490	11.81	0.44
$e^- + C_2H_6 \longrightarrow C_2H_3^+ + H^- + H_2 + e^-$	0.135	14.50	0.12
$e^- + C_2H_6 \longrightarrow C_2H_2^+ + 2\,H_2 + 2\,e^-$	0.080	14.41	0.07
$e^- + C_2H_6 \longrightarrow CH_3^+ + CH_3 + 2\,e^-$	0.032	13.72	0.03

Table 4.5 presents a summary of the possible reactions along with their product distribution and respective reaction rates, for the processes between the ions resulting from primary ionization (Table 4.4) and C_2H_6 molecules, at room temperature.

TABLE 4.5: Possible reactions, product distribution and rate constants for the collisions of the primary ions with C_2H_6. Adapted from [62].

Reaction	Rate Const. (10^{-9} cm^{3}s^{-1})	Prod.Dist.	Ref.
$C_2H_6^+ + C_2H_6 \longrightarrow C_3H_8^+ + CH_4$	0.019 ± 0.001	0.42	[63]
$C_2H_6^+ + C_2H_6 \longrightarrow C_3H_9^+ + CH_3$	0.019 ± 0.001	0.58	[63]
$C_2H_5^+ + C_2H_6 \longrightarrow C_4H_9^+ + H_2$	0.040 ± 0.003	1.00	[63]
$C_2H_4^+ + C_2H_6 \longrightarrow C_3H_6^+ + CH_4$	0.0053 ± 0.0001	0.07	[63]
$C_2H_4^+ + C_2H_6 \longrightarrow C_3H_7^+ + CH_3$	0.0053 ± 0.0001	0.93	[63]
$C_2H_3^+ + C_2H_6 \longrightarrow C_2H_5^+ + C_2H_4$	0.62 ± 0.03	0.47	[63]
$C_2H_3^+ + C_2H_6 \longrightarrow C_3H_5^+ + CH_4$	0.62 ± 0.03	0.40	[63]
$C_2H_3^+ + C_2H_6 \longrightarrow C_4H_7^+ + H_2$	0.62 ± 0.03	0.13	[63]
$C_2H_2^+ + C_2H_6 \longrightarrow C_2H_4^+ + C_2H_4$	1.46 ± 0.06	0.18	[63]
$C_2H_2^+ + C_2H_6 \longrightarrow C_2H_5^+ + C_2H_3$	1.46 ± 0.06	0.09	[63]
$C_2H_2^+ + C_2H_6 \longrightarrow C_3H_3^+ + CH_3 + H_2$	1.46 ± 0.06	0.18	[63]
$C_2H_2^+ + C_2H_6 \longrightarrow C_3H_5^+ + CH_3$	1.46 ± 0.06	0.54	[63]
$C_2H_2^+ + C_2H_6 \longrightarrow C_4H_5^+ + H_2 + H$	1.46 ± 0.05	0.18	[63]
$C_2H_2^+ + C_2H_6 \longrightarrow C_4H_7^+ + H$	1.46 ± 0.06	0.09	[63]
$CH_3^+ + C_2H_6 \longrightarrow C_2H_5^+ + CH_4$	1.74 ± 0.06	0.85	[63]
$CH_3^+ + C_2H_6 \longrightarrow C_3H_5^+ + 2\,H_2$	1.74 ± 0.06	0.09	[63]
$CH_3^+ + C_2H_6 \longrightarrow C_3H_7^+ + H_2$	1.74 ± 0.06	0.06	[63]

From these secondary ions formed, two groups of ions can be identified, these being 3-carbon ($C_3H_n^+$) and 4-carbon ($C_4H_n^+$) ions. However, there is a slight difference

on the ions produced between the pure C_2H_6 [17] and the Xe–C_2H_6 case, which is the supression of $C_2H_3^+$, $C_2H_2^+$ and CH_3^+, resulting mainly in the production of the ions $C_3H_7^+$, $C_3H_8^+$ and $C_3H_9^+$ with 3-carbons and $C_4H_9^+$ and $C_4H_{10}^+$ with 4-carbons.

Furthermore, the relative abundance of these ions is not fully explained by the data in the tables 4.4 and 4.5. In fact, like in the case of pure C_2H_6 [17], this unexpected higher relative abundance of $C_4H_n^+$ (corresponding to a higher peak in the spectrum) can be explained by the reaction involving $C_2H_4^+$ with C_2H_6, since this reaction is incomplete at 293 K (our experimental conditions), and therefore can lead to an intermediary product, $C_4H_{10}^+$, which contributes to the $C_4H_n^+$ peak area instead of the $C_3H_n^+$ one. According to [64], this is a 2-step reaction:

$$C_2H_4^+ + C_2H_6 \longrightarrow C_4H_{10}^+ \tag{4.1}$$

$$C_4H_{10}^+ \longrightarrow C_3H_7^+ + CH_3 \tag{4.2}$$

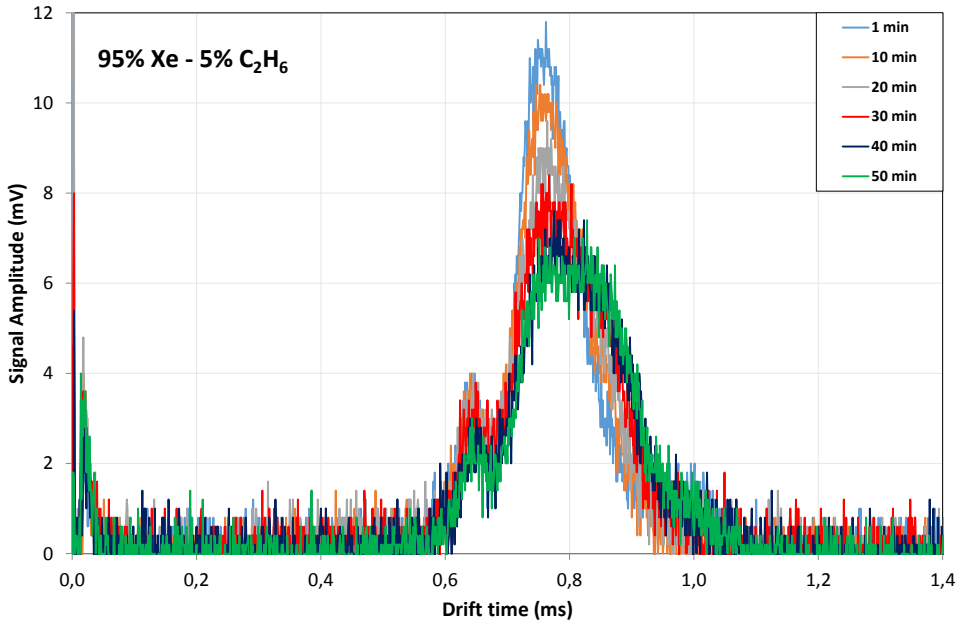

FIGURE 4.4: Time-of-arrival spectra obtained in the degradation study for a mixture of 95% Xe - 5% C_2H_6.

As stated before, for Xe concentrations above 70 % and for reduced electric fields higher than 20 Td, a small peak starts to appear at the right side of the main one. In order to understand, at some extent, the phenonena behind this appearance that

corresponds to an ion with lower mobility, a deterioration study of the signal collected in the grid was performed.

Fig. 4.4 displays the signal degradation to study the ion time-of-arrival spectra for Xe-C_2H_6 mixtures at a pressure of 8 Torr, E/N of 20 Td, voltage across the GEM of 20 V and a temperature of 293 K.

In the fig. 4.4 is seen that for a mixture of 95 % Xe and 5% C_2H_6 and reduced electric fields of 20 Td, the peak with higher mobility, $C_3H_n{}^+$, has a continuous decrease of intensity, which is accompanied with an increase of the drift time, resulting in a decrease of their mobility. A similar behaviour is also observed for the more intense peak. We concluded that leaving the mixture in the chamber, allows the presence of a higher percentage of impurities from outgassing and these impurities might interact with the cations, slowing them down, resulting in a decrease in their mobility and peak intensity. Nevertheless, at the right side of the main peak, the height of the small peak stays almost the same, which implies that this bump did not arise from impurities, this is, the bump does not represent any kind of water ions, or other associated with the presence of impurities.

Even though this test did not allow to correctly identify the nature of the small peak, it provided important information, regarding the effect of impurites.

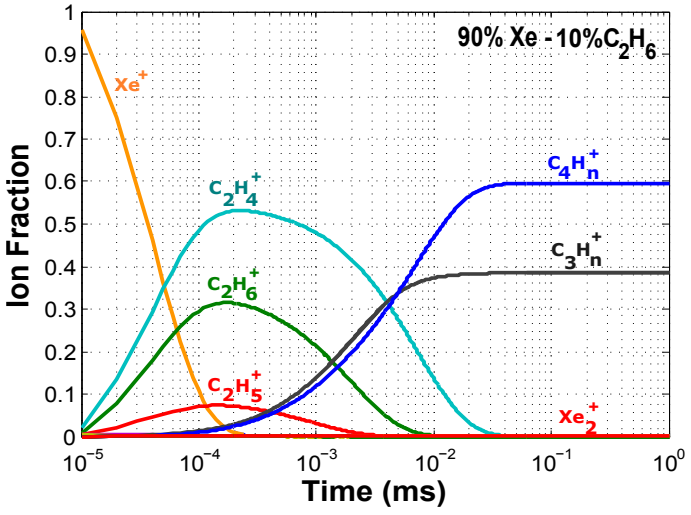

FIGURE 4.5: Fraction of ions that can be formed as a function of time for 90% Xe and 10% C_2H_6 for a pressure of 8 Torr and energy of 20 eV.

Meanwhile, looking at table 4.3, it is possible to see that $Xe_2{}^+$ may react with C_2H_6 resulting in $XeC_2H_6{}^+$, which has a lower mobility than the other ions and could explain the appearance of this peak. In this case, $Xe_2{}^+$ would need to be formed under

these circumstances. Nevertheless, the reaction for the formation of $Xe_2{}^+$ (table 4.2) is much slower than the competitive ones displayed in the table 4.3, so $XeC_2H_6{}^+$ is not expected to be present.

In fig. 4.5 is displayed the evolution of the ions' distribution as a function of time for 90% Xe - 10% C_2H_6. To obtain the fraction of the different ions, the eq. 2.11, introduced previously in section 2.2, was used. Using the reaction rates available in tables 4.2, 4.3, 4.5 and considering the initial fraction of ions approximately the product between the relative pressure for a certain gas and the relative electron impact ionization cross section, defined as:

$$\sigma_{\mathrm{rA}} = \frac{\sigma_{\mathrm{eA}}}{\sigma_{\mathrm{eA}} + \sigma_{\mathrm{eB}}} \tag{4.3}$$

and

$$\sigma_{\mathrm{rB}} = 1 - \sigma_{\mathrm{rA}} \tag{4.4}$$

where in this case A reports to Xenon and B reports to C_2H_6.

The results presented in fig. 4.5 show that for this drift time, in the spectra $t_{DRIFT} = 0.95$ ms, the only ions possible to be observed are $C_3H_n{}^+$ and $C_4H_n{}^+$.

As no alternative reaction was found in literature that justifies the presence of this peak, it was considered that the mechanism responsible for its appearance lies in the resonant charge transfer of $C_2H_6{}^+$ to C_2H_6 [65, 66]. This will affect the mobility of the product ions ($C_3H_8{}^+$ and $C_3H_9{}^+$), slowing them down. As can be seen, increasing Xe concentration will lead to a significant increase in the reaction time of $C_2H_6{}^+$ with C_2H_6, which will contribute to the higher influence of the resonant charge transfer on the overall transit time of $C_3H_8{}^+$ and $C_3H_9{}^+$.

Besides, a shift of the peaks towards lower drift times (increasing mobilities) with decreasing Xe concentration can be observed. This effect can be explained by the lower polarizability of Xe atoms and higher reduced mass involved in the collisions of the ions with Xe atoms which reduces their mobility, as expressed by the Langevin limit formula (eq. 2.15). In order to clarify the ion identification hypothesis given earlier, Blanc's law was used as a cross check method.

Fig. 4.6 shows the inverse reduced mobility of the ions produced in the Xe–C_2H_6 mixture for different mixture ratios for a pressure of 8 Torr and for E/N of 20 Td at room temperature, together with Blanc's law prediction for the main candidate ions - $C_3H_n{}^+$ (orange) and for $C_4H_n{}^+$ (red). For this mixture, K_{g1} and K_{g2} in Blanc's law (eq. 2.17) were obtained either using experimental values from literature or, when not possible, by using the Langevin limit formula (eq. 2.15);

It can be seen in fig. 4.6 that $C_3H_n{}^+$ and $C_4H_n{}^+$ display a small decrease in

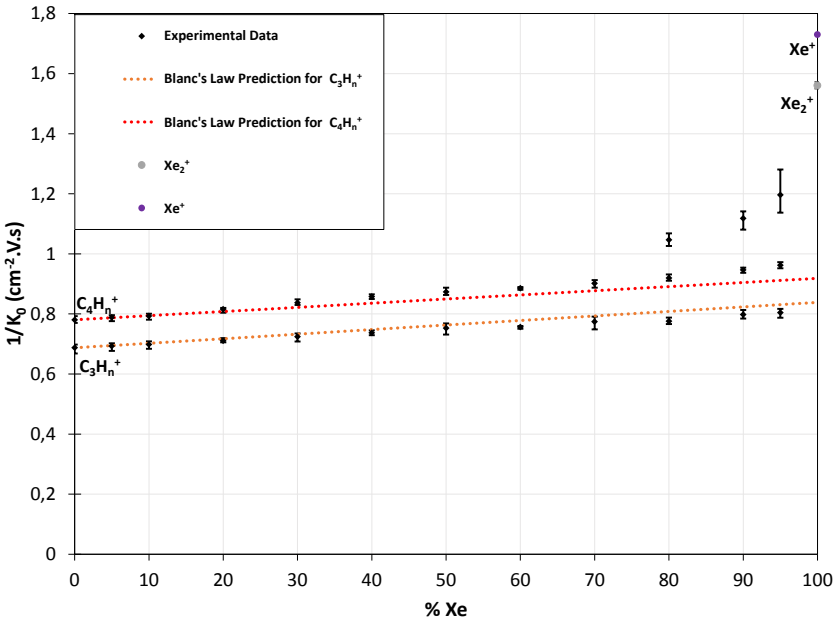

FIGURE 4.6: Inverse reduced mobility of the ions produced in the Xe-C_2H_6 mixture for a pressure of 8 Torr and for a E/N of 20 Td at a room temperature.

mobility as Xe percentage increases, with both being described by Blanc's law. For the third peak, which starts to appear for Xe concentrations above 70%, the mobility was seen to decrease faster than the other peaks. Since the Blanc's law does not account for charge transfer processes, which is assumed to be the process responsible for the formation of the third peak, then due to the limitations already stated in section 2.3.3, Blanc's law fails in describing this case.

Table 4.6 summarizes the results obtained for the mobilities in the range of E/N between (15 - 25 Td) and pressure of 8 Torr.

TABLE 4.6: Mobility of the ions observed for pure Xe and C_2H_6 and Xe-C_2H_6 mixture ratios of 5%, 10%, 20%, 30%, 40%, 50%, 60%, 70%, 80%, 90%, 95% of Xe, obtained for different E/N and a pressure of 8 Torr at room temperature (293 K) and a voltage across the GEM of 20 V.

Mixture	15 Td	20 Td	25 Td	Ion
100% C_2H_6	1.29 ± 0.03	1.28 ± 0.02	1.27 ± 0.03	$\mathbf{C_4H_n}^+$
	1.45 ± 0.03	1.46 ± 0.04	1.43 ± 0.04	$\mathbf{C_3H_n}^+$
5% Xe - 95% C_2H_6	1.28 ± 0.02	1.27 ± 0.02	1.27 ± 0.02	$\mathbf{C_4H_n}^+$
	1.44 ± 0.04	1.44 ± 0.03	1.43 ± 0.04	$\mathbf{C_3H_n}^+$
10% Xe - 90% C_2H_6	1.26 ± 0.02	1.26 ± 0.02	1.25 ± 0.01	$\mathbf{C_4H_n}^+$
	1.42 ± 0.04	1.43 ± 0.03	1.41 ± 0.03	$\mathbf{C_3H_n}^+$
20% Xe - 80% C_2H_6	1.22 ± 0.03	1.23 ± 0.02	1.22 ± 0.02	$\mathbf{C_4H_n}^+$
	1.39 ± 0.04	1.41 ± 0.02	1.38 ± 0.02	$\mathbf{C_3H_n}^+$
30% Xe - 70% C_2H_6	1.20 ± 0.03	1.19 ± 0.02	1.19 ± 0.01	$\mathbf{C_4H_n}^+$
	1.39 ± 0.03	1.38 ± 0.03	1.36 ± 0.03	$\mathbf{C_3H_n}^+$
40% Xe - 60% C_2H_6	1.17 ± 0.02	1.17 ± 0.01	1.16 ± 0.01	$\mathbf{C_4H_n}^+$
	1.35 ± 0.02	1.36 ± 0.02	1.34 ± 0.01	$\mathbf{C_3H_n}^+$
50% Xe - 50% C_2H_6	1.15 ± 0.02	1.14 ± 0.02	1.15 ± 0.04	$\mathbf{C_4H_n}^+$
	1.34 ± 0.04	1.33 ± 0.04	1.31 ± 0.02	$\mathbf{C_3H_n}^+$
60% Xe - 40% C_2H_6	1.13 ± 0.02	1.13 ± 0.01	1.12 ± 0.02	$\mathbf{C_4H_n}^+$
	1.32 ± 0.02	1.32 ± 0.01	1.29 ± 0.03	$\mathbf{C_3H_n}^+$
70% Xe - 30% C_2H_6	-	0.99 ± 0.02	1.01 ± 0.03	-
	1.11 ± 0.02	1.11 ± 0.02	1.10 ± 0.03	$\mathbf{C_4H_n}^+$
	1.30 ± 0.03	1.29 ± 0.04	1.27 ± 0.04	$\mathbf{C_3H_n}^+$
80% Xe - 20% C_2H_6	-	0.96 ± 0.03	0.97 ± 0.04	-
	1.09 ± 0.01	1.09 ± 0.01	1.08 ± 0.01	$\mathbf{C_4H_n}^+$
	1.29 ± 0.01	1.29 ± 0.02	1.26 ± 0.02	$\mathbf{C_3H_n}^+$
90% Xe - 10% C_2H_6	-	0.89 ± 0.07	0.87 ± 0.10	-
	1.06 ± 0.01	1.06 ± 0.01	1.06 ± 0.01	$\mathbf{C_4H_n}^+$
	1.27 ± 0.03	1.25 ± 0.02	1.24 ± 0.02	$\mathbf{C_3H_n}^+$
95% Xe - 5% C_2H_6	-	0.84 ± 0.11	0.81 ± 0.03	-
	1.05 ± 0.02	1.04 ± 0.01	1.04 ± 0.02	$\mathbf{C_4H_n}^+$
	1.25 ± 0.02	1.24 ± 0.03	1.23 ± 0.01	$\mathbf{C_3H_n}^+$
100% Xe	0.65 ± 0.02	0.64 ± 0.01	0.64 ± 0.01	$\mathbf{Xe_2}^+$

4.3.2 Xe-CH_4

We performed also the study of the ion mobility in Xe-CH_4 mixtures. The time of arrival spectra obtained for several Xe-CH_4, averaged to 128 pulses and with the background subtracted, are displayed in fig. 4.7. In xenon-methane ($Xe-CH_4$) mixtures, two distincts groups of ions are observed for all mixture compositions studied, from pure Xe to pure CH_4, as can be seen in fig. 4.7. The ions responsible for the several peaks were found to depend on the mixture ratio, suggesting that they are originated by both CH_4 and Xe.

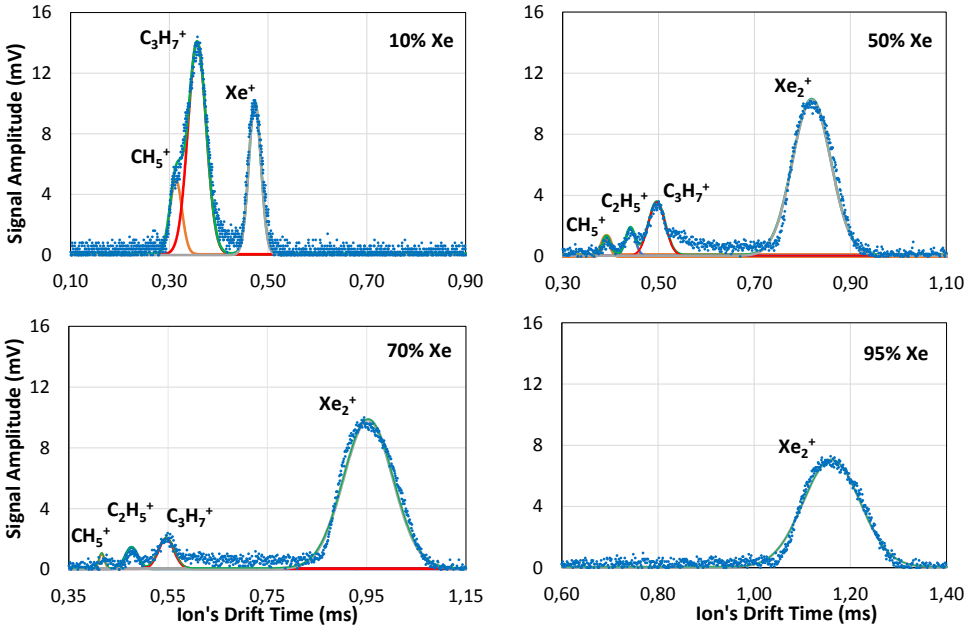

FIGURE 4.7: Time-of-arrival spectra of an average of 128 pulses recorded for several Xe-CH_4 mixtures (10%, 50%, 70% and 95% of Xe) at a pressure of 8 Torr, temperature of 293 K and for a reduced electric field of 20 Td with a V_{GEM} of 20 V.

The evolution of the proportion of the peaks observed (from CH_4 and Xe ions) with the mixture composition can be explained analysing the total cross section for electron impact ionization of Xe (2.43×10^{-16} cm^2 [49]) and CH_4 (1.42×10^{-16} cm^2 [67]), at an electron impact energy of about 20 eV. The ionization probability for Xe is around 1.5 times higher than for CH_4. It is thus expected that, even at lower Xe concentrations (down to 40% of Xe), Xe ions will still be preferentially produced.

Although energetically favoured, references to the charge transfer between CH_4^+ and Xe (eq. 4.5 path (1)) were not found in the literature. The only related reference found was to a charge transfer from a doublet state of Xe^+ to CH_4 (eq. 4.5 path(2)) [68].

Nevertheless, the prevalence of the charge transfer reaction represented by (1) in eq. 4.5 would reinforce the experimental observations justifying the presence and abundance of Xe ions even at low Xe concentrations.

$$CH_4{}^+ + Xe \underset{2}{\overset{1}{\rightleftharpoons}} CH_4 + Xe^+ \tag{4.5}$$

Looking at Fig. 4.7, there are two relevant aspects, both as a result of increasing Xe concentration in the mixture: one is the decrease in mobility of the different ions observed, and the other is the change of the dominant ion species present, which can be identified by a decrease in the area of the group of ions with higher mobility, and an increase in the peak area of the second group of ions, indicating that the faster group of ions are generated from CH_4 molecules while the second, and slower group, is originated by Xe atoms.

As stated before, these faster group of ions are generated from CH_4 molecules. As a matter of fact, table 4.7 summarizes the possible reactions due to electron impact in CH_4 for electron energies of 20 eV, displaying the reactions involving the primary ions.

TABLE 4.7: Ionization reactions, ionization cross sections for electron impact (20 eV) on CH_4 [67], appearance energy (A.E) [69] and respective product distribution.

Reaction	Cross Sec. (10^{-16} cm^2)	A.E. (eV)	Prod. Dist.
$e^- + CH_4 \longrightarrow CH_4{}^+ + 2\,e^-$	0.892	12.65 ± 0.4	62.8 %
$e^- + CH_4 \longrightarrow CH_3{}^+ + H^- + e^-$ $e^- + CH_4 \longrightarrow CH_3{}^+ + H + 2\,e^-$	0.512	13.58 ± 0.1 14.34 ± 0.1	36.0 %
$e^- + CH_4 \longrightarrow CH_2{}^+ + H_2 + 2\,e^-$	0.0169	15.10 ± 0.1	1.2 %

Meanwhile, these primary ions undergo reactions with the molecules of CH_4, forming the secondary ions responsible for the peaks observed in the CH_4 group in fig.4.7. These chemical reactions, involving the primary ions displayed in table 4.7 and CH_4 molecules, with their respective reaction rates and product distributions at room temperature [62], are displayed in table 4.8.

So, according with table 4.8 the fastest ions belong to the group of CH_4 ions, eventually $CH_5{}^+$ (lighter, thus higher mobility), $C_2H_5{}^+$ and $C_3H_7{}^+$ (heavier, thus with lower mobility).

In fig. 4.8 is represented the evolution of the ions distribution as a function of time, for Xe concentrations of 10%, at the left side, and for Xe concentrations of 50% at the right side, obtained through the reaction rates from table 4.2 and 4.8 and through eq. 4.3 , 4.4 and 2.11.

TABLE 4.8: Product distribution and rate constants for the collisions of the primary ions with CH_4. Adapted from [54, 62].

Reaction	Prod. Dist.	Rate Const. ($10^{-9}\,cm^3s^{-1}$)
$CH_4^+ + CH_4 \longrightarrow CH_5^+ + CH_3$	1.00	1.140 ± 0.171
$CH_3^+ + CH_4 \longrightarrow C_2H_5^+ + H_2$	1.00	1.100 ± 0.165
$CH_2^+ + CH_4 \longrightarrow C_2H_4^+ + H_2$ $CH_2^+ + CH_4 \longrightarrow C_2H_5^+ + H$	0.70 0.30	1.300 ± 0.195
$C_2H_5^+ + CH_4 \longrightarrow C_3H_7^+ + H_2$	1.00	0.00009 ± 0.0000135

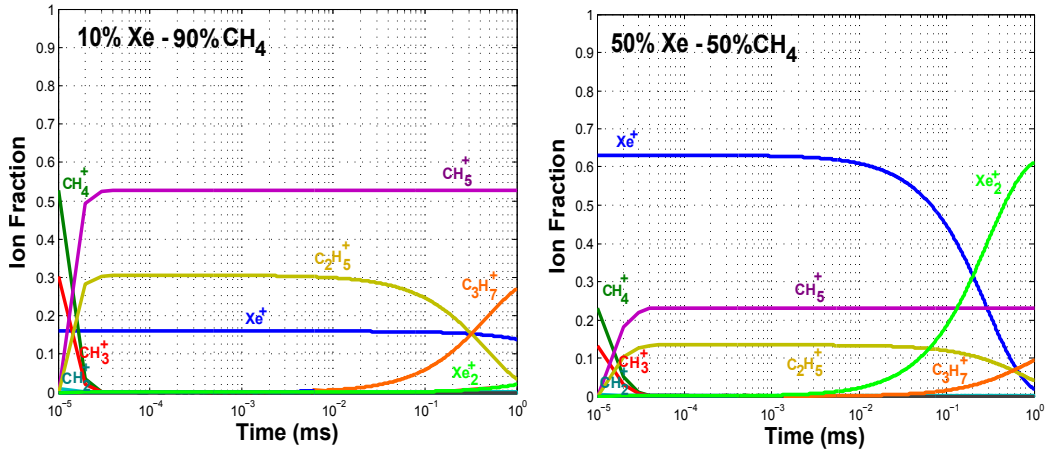

FIGURE 4.8: Fraction of ions that can be formed as a function of time for 10% Xe and 90% CH_4 and 50% Xe and 50% CH_4 for a pressure of 8 Torr and energy of 20 eV, respectively.

According to fig. 4.8, at 10% of Xe, the ions that should be formed after travelling the drift distance (t_{DRIFT} = 0.5 ms) are the ones already mentioned in fig.4.7 at the same conditions, thus CH_5^+, $C_3H_7^+$, Xe^+. However, it is important to point out a deviation for the relative abundance of CH_5^+. Even though, in previous studies using methane [16, 20], the main peak corresponded to this ion, in our espectra that was not the case. At 50% of Xe, the ions formed after crossing the drift distance (t_{DRIFT} = 0.85 ms) are the ones observed at the same conditions in fig. 4.7, thus CH_5^+, $C_2H_5^+$, $C_3H_7^+$ and Xe_2^+. The relative abundance of CH_5^+ remains high in fig. 4.8, but not in fig. 4.7. Futher inspection in the relative abundance of ions confirms an increase of the concentration of Xe ions, adding more Xe in the mixture, which corraborates the spectra obtained. So, regarding the calculus of the reaction time for CH_4, one can only assume that maybe, in the present conditions, are being formed less ions of CH_4^+ than it was expected, due to the presence of some kind of impurities that affect the quantity of CH_4^+

ions through electron impact ionization and so that leads to less ions of this kind in the mixture. Other explanation may be connect with the eq. 4.5 path (1). Since there are no reaction rate values regarding this reaction it is not possible to know the effect of this factor in the fraction of ions, but the substancial decrease of the CH_5^+ peak in fig. 4.7 might be explained through this reaction.

A study of signal degradation was performed, since there were some doubts about the nature of the peaks.

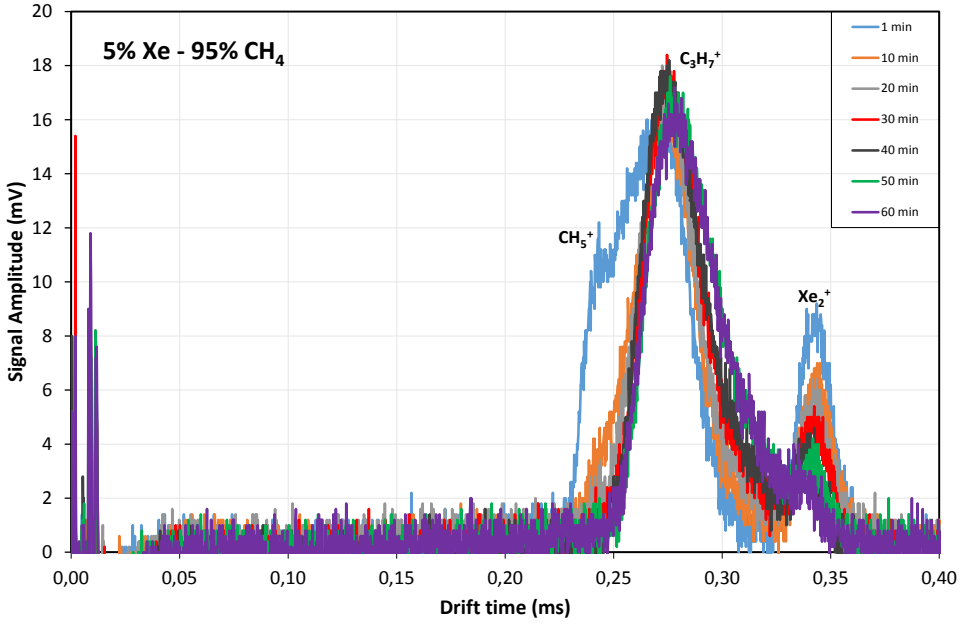

FIGURE 4.9: Time of arrival spectra obtained in the degradation study for a mixture of 5% Xe and 95% CH_4.

Fig. 4.9 displays the signal degradation to study the time-of-arrival spectra for Xe-CH_4 mixtures at a pressure of 8 Torr, E/N of 20 Td, voltage across the GEM of 20 V and a temperature of 293 K. This study displays the time spectra for a mixture of 5% Xe and 95% CH_4.

From fig. 4.9, it is easily understood that none of the peaks was correlated with impurities, namely water ions, since neither of the peaks showed an increase of their intensity, when exposed to higher impurities due to outgassing, instead the intensity of all peaks decreased. Nevertheless, some considerations can be made related with the intensity of the peaks. Starting with CH_5^+ and $C_3H_7^+$, we notice that these peaks show a substancial decrease, especially CH_5^+, disappearing after 40 minutes of data

taking with the same gas filling. So, it seems that maybe impurities slowing down CH_5^+, originating that these ions might be collected almost at the same time as the $C_3H_7^+$, possibly explaining a slight shift towards higher drift times, with also this main peak almost keeping the same area. This explanation related to the slow down of ions by impurities, was a behaviour observed previously at atmospheric pressures [22]. If we reduce the impact of impurities, these problems should be solved.

Focusing on the variation of ions present throughout the mixture, starting from pure CH_4 and up to 5% Xe, only two peaks are observed, being the ions responsible for these peaks connected with two groups identified in pure CH_4: CH_5^+(the peak with higher mobility) and $C_3H_7^+$ (the most intense peak). As mentioned previously, CH_5^+ is originated by CH_4^+ through the following reaction,

$$CH_4^+ + CH_4 \longrightarrow CH_5^+ + CH_3 \tag{4.6}$$

whose probability may be further enhanced by the charge transfer of Xe^+ to CH_4 (eq.4.5 path (2)). The $C_3H_7^+$ ion comes from a two-step reaction [70] (table 4.8):

$$CH_3^+ + CH_4 \longrightarrow C_2H_5^+ + H_2 \tag{4.7}$$

$$C_2H_5^+ + CH_4 \longrightarrow C_3H_7^+ + H_2 \tag{4.8}$$

Increasing Xe concentration from 5% up to 20% results in the rise of a new peak, with lower mobility, at the right side of the $C_3H_7^+$ peak. This peak is related with the availability of Xe, since its area increases with Xe concentration. In this region, Xe^+ is expected to be formed , since the reaction resulting in Xe_2^+ is not yet completed during the drift time of the group of ions.

Between 20% and 80% Xe, in addition to the already mentioned peaks, another one starts to appear at the left side of the $C_3H_7^+$ peak corresponding to $C_2H_5^+$ peak. This ion results from the longer reaction time for the formation $C_3H_7^+$ (eq. 4.8) at lower CH_4 abundance, allowing $C_2H_5^+$ ions to reach the collecting grid. Concerning the Xe ions' group, the increasing concentration of Xe in the mixture will lead to the formation of Xe_2^+, replacing Xe^+.

Finally, for Xe concentration above 80% and up to pure Xe, only one peak is observed, so from the evolution observed, it was attributed to Xe_2^+, with a higher diffusion (broader peak).

In fig. 4.10, it is plotted the inverse of the reduced mobility of the ions produced in Xe-CH_4 mixtures as a function of Xe percentage, for 8 Torr and 20 Td at room

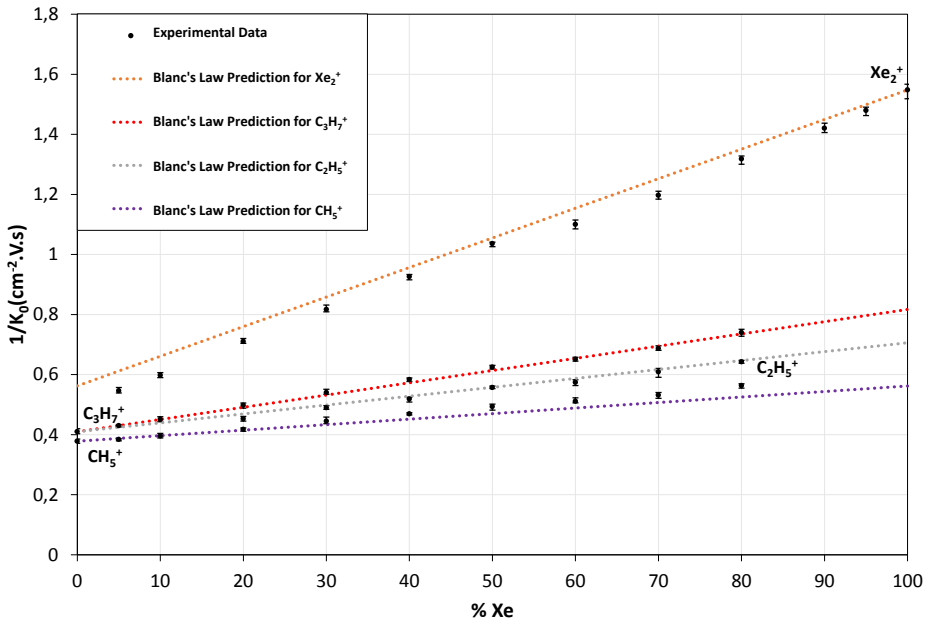

FIGURE 4.10: Inverse reduced mobility of the ions produced in the Xe-CH_4 mixture for a pressure of 8 Torr and for a E/N of 20 Td at room temperature.

temperature (293 K), together with Blanc's law prediction for Xe_2^+ (orange dashed line), CH_5^+ (purple dashed line), $C_2H_5^+$ (grey dashed line) and $C_3H_7^+$ (red dashed line). K_{g1} and K_{g2} in Blanc's law, were obtained using experimental values from the literature or, when not possible, by making use of the Langevin limit (eq. 2.15).

From 100 % down to 20% Xe, in fig. 4.10, the experimental values obtained for the several ions identified follow Blanc's law (eq. 2.17), with the exception of the one for CH_5^+ and Xe_2^+ which deviate from it. In the CH_5^+ case, this can indicate the increasing influence of CH_4^+ in the CH_5^+ drift due to the longer reaction time for the formation of CH_5^+ for Xe percentages above 20%. Since CH_4^+ is likely to be affected by resonant charge transfer to CH_4, this can explain the measured mobility values below the expected by Blanc's law. As for Xe_2^+, whose mobility is seen to be lower than the expected by Blanc's law, one possible explanation for this behaviour is the influence of its predecessor ion, Xe^+, whose mobility is affected by resonant charge transfer, a phenomena not accounted for in Blanc's law.

The ion mobility values measured were seen to vary with the relative abundance of the gases, but no significant variation of the mobility was observed in the range of E/N (10 - 25 Td) studied.

Table 4.9 summarizes the results obtained for the mobilities in the range of E/N between (10 - 20 Td) at pressure of 8 Torr.

From the experimental results and the simulation performed with the reaction path of the relative abundance of the ions, it is possible to conclude that the ions observed depend on the relative abundance of the gases.

TABLE 4.9: Mobility of the ions observed for Xe-CH_4 mixtures obtained for different *E/N*, pressure of 8 Torr at room temperature and a V_{GEM} of 20 V.

Mixture	10 Td	15 Td	20 Td	Ion
100% CH_4	2.52 ± 0.05	2.46 ± 0.06	2.44 ± 0.06	$\mathbf{C_3H_7}^+$
	2.77 ± 0.05	2.67 ± 0.08	2.64 ± 0.05	$\mathbf{CH_5}^+$
5% Xe - 95% CH_4	1.86 ± 0.04	1.85 ± 0.04	1.83 ± 0.04	$\mathbf{Xe}^+$
	2.38 ± 0.05	2.34 ± 0.04	2.33 ± 0.02	$\mathbf{C_3H_7}^+$
	2.68 ± 0.05	2.61 ± 0.04	2.61 ± 0.03	$\mathbf{CH_5}^+$
10% Xe - 90% CH_4	1.69 ± 0.02	1.68 ± 0.04	1.67 ± 0.02	$\mathbf{Xe}^+$
	2.27 ± 0.03	2.23 ± 0.05	2.22 ± 0.04	$\mathbf{C_3H_7}^+$
	2.57 ± 0.04	2.56 ± 0.04	2.53 ± 0.06	$\mathbf{CH_5}^+$
20% Xe - 80% CH_4	1.44 ± 0.02	1.43 ± 0.03	1.41 ± 0.02	$\mathbf{Xe_2}^+$
	2.09 ± 0.03	2.04 ± 0.03	2.01 ± 0.04	$\mathbf{C_3H_7}^+$
	-	2.23 ± 0.04	2.21 ± 0.04	$\mathbf{C_2H_5}^+$
	2.49 ± 0.07	2.43 ± 0.03	2.40 ± 0.03	$\mathbf{CH_5}^+$
30% Xe - 70% CH_4	1.25 ± 0.02	1.24 ± 0.03	1.22 ± 0.02	$\mathbf{Xe_2}^+$
	1.91 ± 0.04	1.87 ± 0.03	1.85 ± 0.04	$\mathbf{C_3H_7}^+$
	2.13 ± 0.06	2.08 ± 0.03	2.04 ± 0.03	$\mathbf{C_2H_5}^+$
	2.33 ± 0.06	2.28 ± 0.03	2.25 ± 0.07	$\mathbf{CH_5}^+$
40% Xe - 60% CH_4	1.10 ± 0.02	1.09 ± 0.01	1.08 ± 0.01	$\mathbf{Xe_2}^+$
	1.76 ± 0.03	1.73 ± 0.03	1.71 ± 0.02	$\mathbf{C_3H_7}^+$
	1.98 ± 0.03	1.93 ± 0.03	1.93 ± 0.04	$\mathbf{C_2H_5}^+$
	2.19 ± 0.04	2.15 ± 0.05	2.13 ± 0.02	$\mathbf{CH_5}^+$
50% Xe - 50% CH_4	0.99 ± 0.02	0.97 ± 0.02	0.97 ± 0.01	$\mathbf{Xe_2}^+$
	1.64 ± 0.04	1.61 ± 0.02	1.60 ± 0.02	$\mathbf{C_3H_7}^+$
	1.85 ± 0.04	1.80 ± 0.07	1.80 ± 0.02	$\mathbf{C_2H_5}^+$
	-	2.05 ± 0.06	2.03 ± 0.05	$\mathbf{CH_5}^+$
60% Xe - 40% CH_4	0.93 ± 0.02	0.91 ± 0.01	0.91 ± 0.01	$\mathbf{Xe_2}^+$
	1.58 ± 0.03	1.54 ± 0.03	1.54 ± 0.02	$\mathbf{C_3H_7}^+$
	1.77 ± 0.03	1.74 ± 0.02	1.74 ± 0.03	$\mathbf{C_2H_5}^+$
	-	1.97 ± 0.06	1.96 ± 0.04	$\mathbf{CH_5}^+$
70% Xe - 30% CH_4	0.85 ± 0.01	0.84 ± 0.01	0.84 ± 0.01	$\mathbf{Xe_2}^+$
	1.48 ± 0.03	1.46 ± 0.02	1.46 ± 0.02	$\mathbf{C_3H_7}^+$
	-	-	1.64 ± 0.05	$\mathbf{C_2H_5}^+$
	-	-	1.88 ± 0.04	$\mathbf{CH_5}^+$
80% Xe - 20% CH_4	0.78 ± 0.01	0.76 ± 0.01	0.76 ± 0.01	$\mathbf{Xe_2}^+$
	1.39 ± 0.02	1.36 ± 0.02	1.35 ± 0.02	$\mathbf{C_3H_7}^+$
	-	-	1.56 ± 0.01	$\mathbf{C_2H_5}^+$
	-	-	1.77 ± 0.02	$\mathbf{CH_5}^+$
90% Xe - 10% CH_4	0.72 ± 0.01	0.71 ± 0.01	0.70 ± 0.01	$\mathbf{Xe_2}^+$
95% Xe - 5% C_2H_6	0.69 ± 0.01	0.68 ± 0.01	0.68 ± 0.01	$\mathbf{Xe_2}^+$
100% Xe	0.67 ± 0.01	0.66 ± 0.01	0.65 ± 0.01	$\mathbf{Xe_2}^+$

Chapter 5

Conclusions

In the present report the results obtained for the reduced mobility of ions originated by electron impact in mixtures based on xenon, like xenon-ethane (Xe-C_2H_6) and xenon-methane (Xe-CH_4) at pressures of 8 Torr, low reduced electric fields (10-25 Td) and different concentrations of mixture were presented. The conclusions for each mixture were made in chapter 4, however the results are summarized in this chapter, as a way to introduce a relation between the values of reduced mobility and the mixtures. In fig. 5.1 it is plotted the percentage of Xe in function of the inverse of the reduced mobility, with the results of the measurements made in this work, together with results obtained previously for Xe$-CO_2$ mixtures [26], in order to withdraw some conclusions regarding these mixtures.

Taking a closer look at this figure, it is possible to see a dependence on the mass of the components of the mixtures. Since these comparison is made within the range of Xe mixtures, one can say that the group of ions concerning the mixture Xe-CH_4 are the ones with the fastest mobilities, although one of these groups of ions does not follow this tendency, since it corresponds to a Xe ion. This conclusion was expected, given the small mass of CH_4, when comparing with C_2H_6 or CO_2. Therefore, the mobility of the ions is correlated with the mass of the gases involved, namely a higher mobility is expected for a lower mass of the additive gas and with the polarizability of the gas molecules.

Looking at fig. 5.1 it is possible to see that the types of ions formed depends on the percentage of Xe in the mixture. This observation is relevant for the case of Xe-CO_2 and Xe-CH_4. In Xe-CO_2 the ion responsible for the peak observed changes with the increase of Xe concentration. Regarding the case of Xe-CH_4, it is seen that the number of peaks changes with the Xe concentration and also the ions responsible for the peaks observed.

Of these three mixtures studied, it should be noted that the best mixture for mobility is Xe-C_2H_6. Fig. 5.1 shows that for this mixture the mobility values display

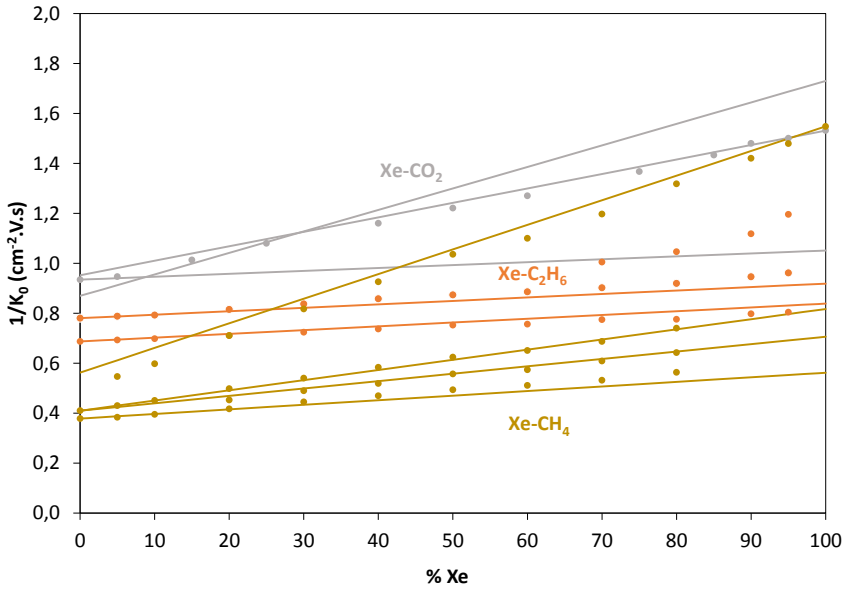

FIGURE 5.1: Compilation of ion mobillity studies on Xenon mixtures.

lower dispersion, when compared the other mixtures, namely Xe-CH_4, where the peak attributed to Xe_2^+ exhibits values of mobilities quite different from the other ions seen for the same mixture. Regarding the Xe-CO_2 it shows lower mobility when compared with the Xe-C_2H_6 mixture, considering the detector's region of interest, about 10% of additive.

Througout this study it was seen that the mobilities measured for these three mixtures did not exhibit a significant dependence with the reduced electric field (E/N) range in which these studies were performed (10 - 25 Td).

Chapter 6

Future Work

6.1 Mixtures of pratical relevance

As mentioned previously, radiation detection uses extensively gas-filled detectors, and their study is necessary to improve the energy resolution, dead time and detection range among others.

In fact, certain parameters may influence the choice of the gas mixture to be used, among these the ions' and electrons' velocity for a wide range of E/N values, the Townsend coefficient, the attachment and diffusion coefficients [46].

The goal of LIP Coimbra is to extend the study on the ion mobility for gas mixtures of pratical use in gaseous detectors. These following mixtures represent the future investigations in the scope of ion mobility studies that will be carried out in our experimental setup:

- **Mixtures of Xe-CF_4**
- **Mixtures of Ar-CO_2-N_2**
- **Mixtures of Xe-CO_2-N_2**
- **Mixtures of Ne-CF_4**
- **Mixtures of Ar-CF_4**
- **Mixtures of Ar-CF_4-Isobutane**

6.2 Optimization of the detector

In science there is a continuous pursuit for improved experimental systems, so that more precise and exact measurements can be obtained, or so that new functions can be added, allowing a deeper and more complex analysis and understanding of physical phenomena.

From my experience, it was easily concluded that some features could be enhanced in the experimental system, identifying in this case its imperfections and ways to solve them. For that reason, the main aspects worthy of reflection for this setup are here discussed.

As already pointed out in chapter 4, the problem of impurities affects the performance of the detector, more precisely the precision of the mobility measurements. So, the solution discussed was heating the walls of the detector. Concerning this solution some problems arise, due to glues and solders, which are not very resistant to high increase temperature. Eventually the use of purifiers inside or when introducing the gas in the IDC should be considered.

Altough this system was also designed with the purpose of being able to calculate the longitudinal diffusion coefficient along with the diffusion of atomic ions and dimer ions in rare gases, until now this measurement was not achievable with great precision, due to the fact that such parameter is highly affected by the conversion rate of the atomic ion into the dimer ion, the space-charge effects and the presence of impurities [4].

Introducing a variable drift distance would lead to a major upgrade in the system. For instance, it will ensure that ions will attain steady drift conditions, while working at very low pressures and high values of electric fields (E/N), since an increase of the drift distance will allow enough collisions with the gas atoms. Other feature that will improve is the resolution of the detector, which should admit a detection of lighter ions and therefore faster ions preventing the ions' signal to be overlapped by the electronic noise.

Given the fact that data on ionic mobility is scarce, even more for negative mobility ions, the detection of negative ions would proportionate an additional feature for this system.

These modifications are planned to be introduced in the near future and should allow to obtain more complete results of the ion mobility.

Bibliography

[1] G.A. Eiceman, Z. Karpas, and H. H. J. Hill, *Ion Mobility Spectrometry*, CRC Press-Taylor & Francis Group, third ed., 2014.

[2] P. Langevin, *Une formule fondamentale de théorie cinetique*, *Annal.Chimie Physique* **5** (1905) 245.

[3] E.A. Mason, E.W. McDaniel, *Transport Properties of Ions in Gases*, John Wiley and Sons, Inc., New York 1988.

[4] P.N.B. Neves, *Studies on the mobility of monoatomic and dimer noble gas ions in their parent gas*. PhD thesis, Universidade de Coimbra, 2009.

[5] A.M. Tyndall, *The Mobility of Positive Ions in Gases*, Cambridge University Press, 1938.

[6] L.B. Loeb, *Basic processes of gaseous electronics*. University of California Press, 1955.

[7] E.W. McDaniel and L.A. Viehland, *The Transport of Slow Ions in Gases: Experiment, Theory and Application*, *Physics Reports (Physics Letters)*, vol.110, no.5/6,pp.333-367, 1984.

[8] H.W. Ellis, R.Y. Pai, E.W. McDaniel, E.A. Mason, L.A. Viehland, *Transport Properties of Gaseous Ions Over a Wide Energy Range*, *Atomic Data and Nuclear Data Tables*, vol.17, pp.117-210, 1976.

[9] H.W. Ellis, E.W. McDaniel, D.L. Albritton, L.A. Viehland, S.L. Lin, E.A. Mason, *Transport Properties of Gaseous Ions Over a Wide Energy Range, Part II*, *Atomic Data and Nuclear Data Tables*, vol.22, pp.179-217, 1978.

[10] H.W. Ellis, M.G. Thackston, E.W. McDaniel, E.A. Mason, *Transport Properties of Gaseous Ions Over a Wide Energy Range. Part III*, *Atomic Data and Nuclear Data Tables*, vol.31, pp.113-151, 1984.

[11] L.A. Viehland, E.A. Mason, *Transport Properties of Gaseous Ions Over a Wide Energy Range, IV*, *Atomic Data and Nuclear Data Tables*, vol.60, pp.37-95, 1995.

[12] S. Armenta, M. Alcala and M. Blanco, *A review of recent unconventional applications of ion mobility spectrometry (IMS)*, *Analytica Chimica Acta*, vol.703, pp.114-123, 2011.

[13] P.N.B. Neves, C.A.N. Conde and L.M.N. Távora *Experimental measurements of the mobilities of atomic and dimer Ar, Kr and Xe ions in their parent gases*, *J. Chem. Phys.*, **133** (2010) 124316.

[14] P.N.B. Neves, A.N.C. Garcia, A.M. Trindade, J.A.S. Barata, L.M.N. Távora and C.A.N. Conde, *Experimental measurements of the Ne^+ and $Ne_2{}^+$ mobilities in Ne ant the reaction rate coefficient for* $\mathrm{Ne}^+ + 2\,\mathrm{Ne} \longrightarrow \mathrm{Ne_2}^+ + \mathrm{Ne}$, *IEEE Trans. Nucl. Sci.*, **58** (2011) 2060.

[15] A.N. Garcia, P.N.B. Neves, A.M.F. Trindade, F.P. Santos and C.A.N. Conde, *A new contribution to the experimental measurement of the mobility of the $N_4{}^+$ and $N_2{}^+$ ion mobility in N_2 at 298K* , *Jinst* **7** (2012) P02012.

[16] A.M.F. Trindade, J. Escada, P.N.B. Neves, T.H.V.T. Dias, J.A.S. Barata, F.P.Santos and C.A.N. Conde, *Experimental measurement of the mobility of methane ions in methane*, *Jinst* **7** (2012) P06010.

[17] A.F.V. Cortez, A.N.C. Garcia, P.N.B. Neves, F.P. Santos, F.I.G.M. Borges, J.A.S. Barata and C.A.N. Conde, *Experimental measurement of the mobility of ions originated in ethane in their parent gas*, *Jinst* **8** (2013) P07013.

[18] A.F.V. Cortez, A.N.C. Garcia, P.N.B. Neves, F.P. Santos, F.I.G.M. Borges, J.A.S. Barata and C.A.N. Conde, *Experimental ion mobility measurements in Ar-C_2H_6*, *Jinst* **8** (2013) P12012.

[19] A.N.C. Garcia, P.N.B. Neves, A.M.F. Trindade, A.F.V. Cortez, F.P. Santos and C.A.N. Conde, *Experimental measurements of the mobility of Xenon-Neon mixtures*, *Jinst* **9** (2014) P07008.

[20] A.M.F. Trindade, A.F.V. Cortez, P.N.B. Neves, A.N.C. Garcia, J. Escada, F.P. Santos and C.A.N. Conde, *Experimental study on ion mobility in Ar-CH_4*, *Jinst* **9** (2014) P06003.

[21] P.M.C.C. Encarnação, A.F.V. Cortez, M.G.A. Pinto, P.N.B. Neves, A.M.F. Trindade, J. Escada, F.P. Santos, F.I.G.M. Borges, J.A.S. Barata and C.A.N. Conde, *Experimental ion mobility measurements in Ar-CO_2*, *Jinst* **10** (2015) P01010.

[22] Y. Kalkan, M. Arslandock, A.F.V. Cortez, Y. Kaya, I. Tapan and R. Veenhof, *Cluster ions in gas-based detectors*, *Jinst* **10** (2015) P07004.

[23] P.M.C.C. Encarnação, A.F.V. Cortez, R. Veenhof, P.N.B. Neves, F.P. Santos, A.M.F. Trindade, F.I.G.M. Borges and C.A.N. Conde, *Experimental ion mobility measurements in Ne-CO_2 and CO_2-N_2 mixtures*, *Jinst* **11** (2016) P05005.

[24] A.F.V. Cortez, P.M.C.C. Encarnação, R. Veenhof, P.N.B. Neves, F.P. Santos, F.I.G.M. Borges and C.A.N. Conde, *Experimental ion mobility measurements in Ne-N_2*, *Jinst* **11** (2016) P11019.

[25] A.F.V. Cortez, P.M.C.C. Encarnação, R. Veenhof, P.N.B. Neves, F.P. Santos, F.I.G.M. Borges and C.A.N. Conde, *Experimental ion mobility measurements in Ne-N_2*, *Jinst* **11** (2016) P11019.

[26] A.F.V. Cortez, M.A.G. Santos, R. Veenhof, R.N. Patra, P.N.B. Neves, F.P. Santos, F.I.G.M. Borges and C.A.N. Conde, *Experimental ion mobility measurements in Xe-CO_2*, *Jinst* **12** (2017) P06012.

[27] A.M.F. Trindade, P.M.C.C. Encarnação, J. Escada, A.F.V. Cortez, P.N.B. Neves, C.A.N. Conde, F.I.G.M. Borges and F.P. Santos, *Experimental ion mobility measurements in xenon-trimethylamine mixtures*, *Jinst* **12** (2017) P07007.

[28] J.M.C. Perdigoto, A.F.V. Cortez, R. Veenhof, P.N.B. Neves, F.P. Santos, F.I.G.M. Borges and C.A.N. Conde, *Experimental ion mobility measurements in Xe-CH_4*, *Jinst* **12** (2017) P09003.

[29] J.M.C. Perdigoto, A.F.V. Cortez,R. Veenhof, P.N.B. Neves, F.P. Santos, F.I.G.M. Borges and C.A.N. Conde, *Experimental ion mobility measurements in Xe-C_2H_6*, accepted for publication.

[30] R.R. Teachout and R.T. Pack, *The static dipole polarizabilities of all the neutral atoms in their ground states*, *Atomic Data and Nuclear Data Tables 3*, (1971) 195-214.

[31] J.O. Hirschfelder, C.F. Curtis and R.B. Bird, *Molecular Theory of Gases and Liquids*, John Wiley and Sons, Inc., New York 1954, p.950 Fundamental information on molecualar polarizabilities.

[32] J.A. Hornbeck, *The Drift Velocities of Molecular and Atomic Ions in Helium, Neon and Argon*, *Physical Review Second Series*, vol.84, no.4, pp.610-615, 1951.

[33] A. Blanc, *Recherches sur la mobilités des ions dans les gaz*, *J. Phys. Theor. Appl.* **7**, (1908) 825-839.

[34] S. Bachmann, A. Bressan, L. Ropelewski, A. Sharma and D. Mo, *Charge amplification and transfer processes in the gas electron multiplier*, *Nuclear Instruments and Methods in Physics Research A*, vol.438, p.376-408, 1999.

[35] P.M.C.C. Encarnação, *Ion Mobility Studies Mixtures used in gas detectors*. MSc thesis, Universidade de Coimbra, 2016.

[36] Edwards Pump Station [online]. Available at mmrc.caltech.edu/Vacuum/Edwards/EXPT20Pumping20Station/EDWARDS%20PUMP%20STATION%20INSTRUCTIONS.pdf.

[37] WRG-S-NW25 [online]. Available at shop.edwardsvacuum.com/products/d14701000/view.aspx.

[38] Edwards Barocel Pressure Sensor 600AB Trans 1000TR [online]. Available at saba.kntu.ac.ir/eecd/Ecourses/instrumentation/projects/reports/Poly20Vaccum/BEdwards/Barocel_600.pdf.

[39] Xenon Gas Container [online]. Available at lindecanada.com/internet.lg.lg.can/en/images/inde_Scientific_Catalogue_0315135_94035.pdf?v=11.0.

[40] Carbon-Dioxide Gas Container [online]. Available at praxair.com/-/media/documents/specification-sheets-and-brochures/gases/carbon-dioxide/carbon-dioxide-co2-spec-sheet-ss-p4574.pdf.

[41] Nitrogen Gas Container [online]. Available at linde-gas.pt/internet.lg.lg.prt/pt/images/Azoto%20comprimido310_81677.pdf?v=4.0.

[42] Argon Gas Container [online]. Available at linde-gas.pt/internet.lg.lg.prt/pt/images/Argon%20comprimido310_81671.pdf?v=4.0.

[43] Ethane Gas Container [online]. Available at praxair.com/-/media/documents/specification-sheets-and-brochures/gases/ethane-c2h6-spec-sheet-ss-p4592.pdf.

[44] Methane Gas Container [online]. Available at read.dmtmag.com/i/25778-specialty-gases-reference-guide/4.

[45] K. Ezaki, K. Akaishi, Y. Kubota and O. Motojima, *Experimental study on scalling law of outgassing rate with a pumping parameter*, *Journal of Vacuum Science & Technology A*, vol.15, p.258-264, 1997.

[46] Y. Assran, A. Sharma, *Transport Properties of operational gas mixtures used at LHC*, *CERN CH1211 Geneve, Switzerland*, 1-36.

[47] B. Dolgoshein, *Transition radiation detectors*, *Nucl. Instrum. Meth. A*, **326** (1993) 434-469 .

[48] A. Andronic, J. P. Wessels, *Transition radiation detectors*, *Nucl. Instrum. Meth. A*, **666** (2012) 130-147.

[49] R. Rejoub, B.G. Lindsay and R.F. Stebblings, *Determination of the absolute partial and total cross sections for electron-impact ionization of the rare gases*, *Phys. Rev. A*, *65* (2002) 042713

[50] B. Gstir, S. Denifl, G. Hanel, M. Rummele, T. Fiegele, P. Cicman, M. Stano, S. Matejcik, P. Scheier, K. Becker, A. Stamatovic and T.D. Mark, *Electron impact multiple ionization of neon, argon and xenon atoms close to threshold:appearance energies and Wannier exponents*, *J. Phys. B: At. Mol. Opt. Phys.* **35**, (2002) 2993-3007.

[51] H. von Köding, F.A. Pinkse and N.M.M. Nibbering, *Rate Coefficients of Single and Double Electron Tranfer from Xe to Xe_2^+ at Low Collision Energies as Determined by Use of Fourier Transform Ion Cyclotron Resonance Mass Spectrometry*, *Physica Scripta. T59* (1995) 418-422.

[52] A.P. Vitols and H.J. Oskam, *Reaction rate constant for $Xe^+ + 2\,Xe \longrightarrow Xe_2^+ + Xe$*, *Phys. Rev. A*, *8* (1973) 1860-1863

[53] Y. Itikawa, *Cross Sections for Electron Collisions with Carbon Dioxide*, *J. Phys. Chem. Ref. Data*, *31(3)* (2002) 749-767

[54] Vicent G. Anicich, *Evaluated Bimolecular Gas Phase Kinetics of Positive Ions for Use in Modeling Planetary Atmospheres, Cometary Comae and Interstellar Clouds*, *J. Phys. Chem.* 22, 6 (1993)

[55] A.B. Rashit and P.Werneck, *Rate Coefficients and Product Ion Distribution for Reactions of $CO_2 \cdot CO_2^+$ Ions with Neutral Molecules at 300K*, *Z. Naturforsch*, *34a* (1979) 1410.

[56] M. Durop-Fergunson, H. Bohringer, D.W. Fahey, E.E. Fergunson, *Enhancement of charge transfer reaction rate constants by vibrational excitation at Kinetic energies below 1 eV*, *J. Chem. Phys.*, *79*, (1983) 265.

[57] Y. Kalkan, M. Arslandok, A.F.V. Cortez, Y. Kaya, I. Tapan and R. Veenhof *Cluster ions in gas-based detectors*, *Journal Instrumentation vol.10* (2015) P01010.

[58] H.W. Ellis, R.Y. Pai, E.W. McDaniel, L.A. Viehland and E.A. Mason, *Transport Properties of Gaseous Ions over a Wide Energy Range*, *Atomic Data Nuclear Data Tables*, *vol.60*, (1995) 35-217.

[59] Cechan Tian and C.R. Vidal, *Electron impact dissociative ionization of ethane: Cross sections, appearance potentials and dissociation pathways*, *Journal Chemical Physics 109(5)*, (1998) 1704-1712.

[60] E. Vašeková, M. Stano, Š. Matejčík, J.D. Skalný, P. Mach, J. Urban, T.D. M *ddotar*k, *Electron impact ionization of C_2H_6: ionization energies and temperature effects*, *International Journal of Mass Spectrometry 235*, (2004) 155-162.

[61] K. Giles, N.G. Adams and D.Smith *Reactions of Kr^+, Kr_2^+, Xe^+, Xe_2^+ ions with several molecular gases at 300K*, *Journal of Physics B: Atomic, Molecular and Optical Physics 22*, (1989) 873-883.

[62] W.T. Huntress Jr., *Laboratory studies of bimolecular reactions of positive ions in interstellar clouds, in comets and in planetary atmospheres of reducing composition*, *Astrophysical Journal Supplement Series 33*, (1977) 495-514.

[63] J.K. Kim, V.G. Anicich, W.T. Huntress Jr., *Product distributions and rate constants for the reactions of CH_3^+, CH_4^+,$C_2H_2^+$, $C_2H_3^+$, $C_2H_4^+$, $C_2H_5^+$, $C_2H_6^+$, Journal of Physical Chemistry 81(19)*, (1977) 1798-1805.

[64] K. Hiraoka and P. Kebarle, *Ion molecule reactions in ethane. Thermochemistry and structures of the intermediate complexes: $C_4H_{11}^+$ and $C_4H_{10}^+$ formed in the reactions of $C_2H_5^+$ and $C_2H_4^+$ with C_2H_6*, *Canadian Journal of Chemistry 58*, (1980) 2262.

[65] E.W. McDaniel, J.B.A. Mitchell, M.E. Rudd, *Atomic collisions- heavy particle projectiles*, *Wiley* (1993) pp.498.

[66] S.K. Searles, L.Wayne Sieck and P. Ausloos, *Reactions of $C_2H_6^+$: Formation of the $(C_2H_6)_2^+$ Ion*, *The Journal of Chemical Physics* 53, 849 (1970).

[67] H.C. Straub, D. Lin, B.G. Lindsay, K. A. Smith and R.F. Stebbings ,*Absolute partial cross sections for electron-impact ionization of CH_4 from threshold to 1000 eV*, *The Journal of Chemical Physics* 106, 4430 (1997).

[68] N.G. Adams, D.Smith, E. Alge *Reactions of the $^2P_{3/2}$ and $^2P_{1/2}$ doublet ground states of Kr^+, Xe^+ at 300K*, *Journal of Physics B: Atomic, Molecular Physics 13*, (1980) 3235-3246.

[69] M. Stano, Š. Matejčík, J.D. Skalný and T.D. Märk, *Electron impact ionization of CH_4: ionization energies and temperature effects*, *Journal of Physics B: Atomic, Molecular and Optical Physics* 36 (2003) 261-271.

[70] K. Hiraoka and P. Kebarle, *Temperature dependence of bimolecular ion molecule reactions. The reaction $C_2H_5^+ + CH_4 = C_3H_7^+ + H_2$*, *The Journal of Chemical Physics* 63, 394 (1975).

[71] M. Saporoschenko, *Mobilities of secondary and tertiary positive ions in methane gas*, *International Journal of Mass Spectrometry and Ion Physics* 42 (1982) 285-294.

Appendix A

Data Compilation

A.1 Ar-N_2

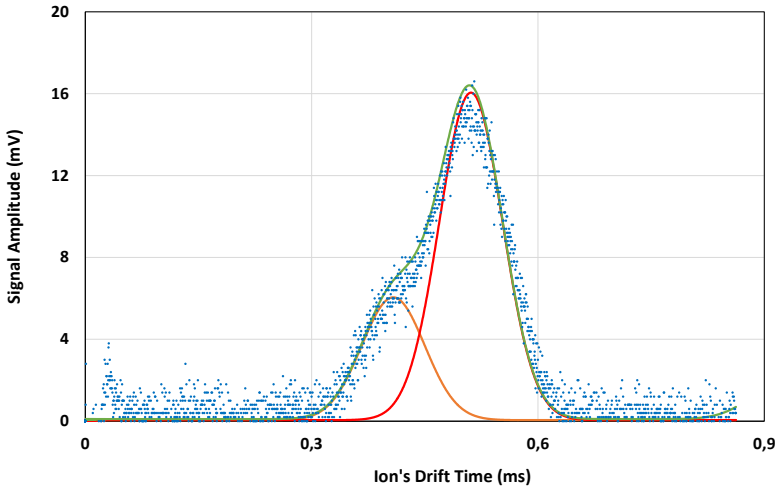

FIGURE A.1: Time of arrival spectra for 95% Ar - 5% N_2 at a pressure of 8 Torr and for a reduced electric field of 15 Td with a voltage across the GEM of 25V at a room temperature

TABLE A.1: Mobility of the ions observed for the Ar-N_2 mixture ratios of 1%, 3%, 5%, 10%, 20%, 30%, 40%, 50%, 60%, 70%, 80%, 90%, 95%, 97% and 99% of Ar, obtained for different E/N and a pressure of 8 Torr at room temperature (298 K) and a voltage across the GEM of 25V.

Mixture	Mobility ($cm^2V^{-1}s^{-1}$)		Ion
	15 Td	20 Td	
100% N_2	2.394 ± 0.039	2.393 ± 0.048	N_4^+
1% Ar - 99% N_2	2.352 ± 0.02	2.330 ± 0.019	N_4^+
3% Ar - 97% N_2	2.291 ± 0.022	2.279 ± 0.010	N_4^+
5% Ar - 95% N_2	2.232 ± 0.025	2.228 ± 0.043	N_4^+
10% Ar - 90% N_2	2.203 ± 0.022	2.192 ± 0.012	N_4^+
20% Ar - 80% N_2	2.217 ± 0.016	2.197 ± 0.010	?
30% Ar - 70% N_2	2.584 ± 0.089	2.452 ± 0.034	H_2O^+
	2.184 ± 0.029	2.163 ± 0.034	?
40% Ar - 60% N_2	2.505 ± 0.085	2.474 ± 0.054	H_2O^+
	2.196 ± 0.020	2.166 ± 0.021	?
50% Ar - 50% N_2	2.591 ± 0.024	2.450 ± 0.075	H_2O^+
	2.176 ± 0.030	2.132 ± 0.052	?
60% Ar - 40% N_2	2.574 ± 0.065	2.490 ± 0.046	H_2O^+
	2.179 ± 0.016	2.139 ± 0.013	?
70% Ar - 30% N_2	2.595 ± 0.098	2.495 ± 0.048	H_2O^+
	2.164 ± 0.025	2.119 ± 0.019	?
80% Ar - 20% N_2	2.618 ± 0.108	2.533 ± 0.052	H_2O^+
	2.153 ± 0.018	2.111 ± 0.018	?
90% Ar - 10% N_2	2.623 ± 0.121	2.514 ± 0.034	H_2O^+
	2.119 ± 0.038	2.096 ± 0.016	?
95% Ar - 5% N_2	2.600 ± 0.078	2.453 ± 0.042	H_2O^+
	2.086 ± 0.031	2.060 ± 0.019	Ar_2^+
97% Ar - 3% N_2	2.490 ± 0.068	2.386 ± 0.060	H_2O^+
	2.056 ± 0.012	2.015 ± 0.014	Ar_2^+
99% Ar - 1% N_2	2.386 ± 0.021	2.372 ± 0.047	H_2O^+
	2.017 ± 0.013	1.978 ± 0.010	Ar_2^+
100% Ar	1.974 ± 0.026	1.954 ± 0.012	Ar_2^+
	1.581 ± 0.020	1.569 ± 0.021	Ar^+